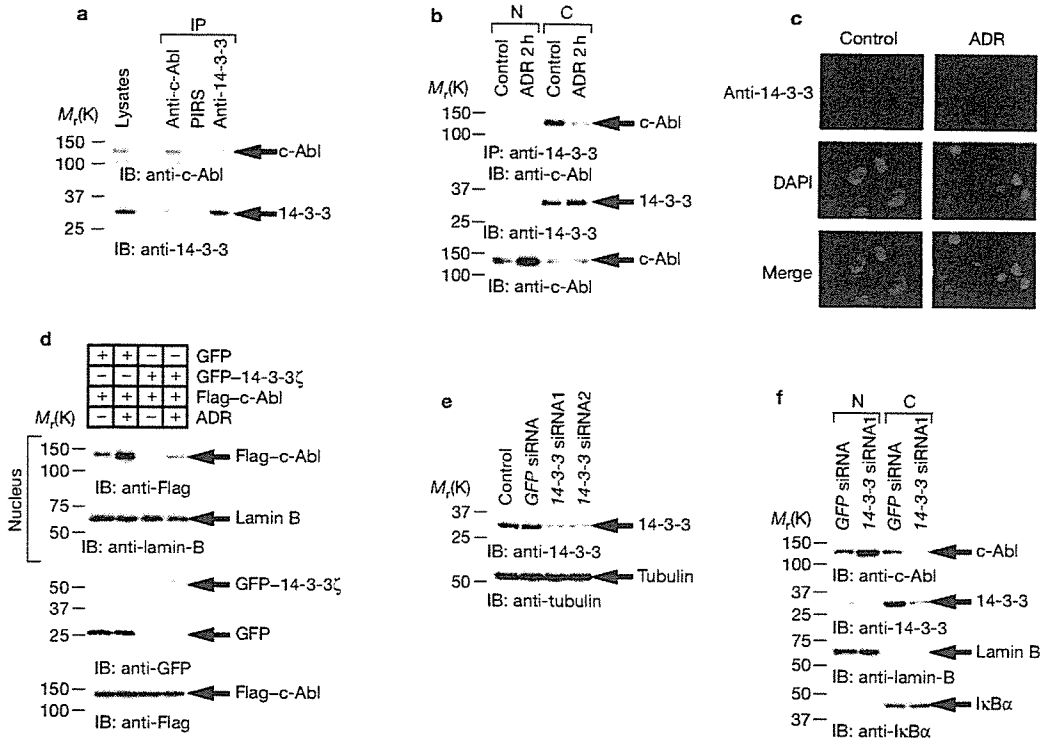

Figure 2 c-ABL interacts with 14-3-3 proteins in the cytoplasm. (**a**) Lysates from HeLa cells were subjected to immunoprecipitation (IP) with pre-immune rabbit serum (PIRS), anti-c-ABL or anti-14-3-3. Cell lysates and immunoprecipitates were analysed by immunoblotting (IB) with anti-c-ABL (upper panel) or anti-14-3-3 (lower panel). (**b**) HeLa cells were treated with adriamycin (ADR) for 2 h. Nuclear (N) and cytoplasmic (C) lysates were subjected to immunoprecipitation with anti-14-3-3 and then immunoblot analysis with anti-c-ABL (upper panel). Lysates were also analysed by immunoblotting with anti-14-3-3 (middle panel) or anti-c-ABL (lower panel). (**c**) HeLa cells were left untreated or were treated with ADR for 2 h. Cells were fixed and stained with anti-14-3-3. Nuclei were stained with DAPI (4',6-diamidino-2-phenylindole). (**d**) 293T cells were transfected with Flag-c-ABL and green fluorescent protein (GFP) vector or GFP–14-3-3ζ. After 2 h treatment with ADR, nuclear lysates were analysed by immunoblotting with anti-Flag (top panel) or anti-lamin-B (second panel). Whole-cell lysates were subjected to immunoblot analysis with anti-GFP (third panel) or anti-Flag (bottom panel). (**e**) HeLa cells were left untransfected (control) or were transfected with GFP small interfering RNA (GFPsiRNA), 14-3-3siRNA1, or 14-3-3siRNA2. Cell lysates were analysed by immunoblotting with anti-14-3-3 (upper panel) or with anti-tubulin (lower panel). (**f**) HeLa cells were transfected with GFPsiRNA or 14-3-3siRNA1. Nuclear and cytoplasmic lysates were subjected to immunoblot analysis with the indicated antibodies.

and an increase in nuclear c-Abl (Fig. 2f). These findings indicate that 14-3-3 proteins sequester c-Abl into the cytoplasm.

14-3-3 proteins bind to a consensus RSXpS/TXP motif and interfere with nuclear import of binding proteins by blocking their NLSs[15,16]. The c-Abl RSVT735LP sequence conforms to the consensus 14-3-3 binding site (Fig. 3a). To determine whether or not c-Abl is phosphorylated on Thr 735, lysates were immunoblotted with an anti-pThr^{735} antibody. Phosphorylation of Thr 735 was detectable in control and ADR-treated cells, indicating that this modification is independent of DNA damage (see Supplementary Information, Fig. S2a). To examine the possibility that phosphorylation of c-Abl on Thr 735 is altered by intracellular translocation of c-Abl in response to DNA damage, nuclear and cytoplasmic lysates were immunoblotted with anti-c-Abl and anti-pThr^{735} antibodies. The findings that the level of c-Abl phosphorylation on Thr 735 parallels that of c-Abl expression in the nucleus and cytoplasm, indicate that this phosphorylation is independent of intracellular c-Abl localization (see Supplementary Information, Fig. S2b). Mutation of c-Abl Thr 735 to Ala abrogated reactivity with anti-pThr^{735} and binding to 14-3-3ζ (Fig. 3b). Binding of c-Abl to 14-3-3σ was also abrogated by the T735A mutation (see Supplementary Information, Fig. S2c). Consistent with these results, c-Abl^{T735A} localized to the nucleus in control and ADR-treated cells (Fig. 3c–e). These findings indicate that 14-3-3 proteins bind to c-Abl at the RSVpTLP motif and thereby sequester c-Abl into the cytoplasm. To further determine if phosphorylation of c-Abl on Thr 735 modulates c-Abl kinase activity, anti-Flag immunoprecipitates of Flag–c-Abl and Flag–c-Abl^{T735A} were analysed for phosphorylation of GST-Crk(120-225) (Fig. 3c). The demonstration that kinase activity of the c-Abl^{T735A} mutant is similar to that of wild-type c-Abl in both control and ADR-treated cells indicates that phosphorylation on Thr 735 is independent of c-Abl kinase activity.

The c-Jun N-terminal kinase (Jnk) protein is activated in the cellular response to DNA damage and phosphorylates 14-3-3ζ on Ser 184 as a mechanism for the release of BAX to mitochondria[17]. To determine whether Jnk regulates the association of c-Abl and 14-3-3 proteins, cells were pretreated with the Jnk inhibitor, SP600125, and then exposed to ADR. Inhibition of Jnk attenuated ADR-induced dissociation of c-Abl from 14-3-3 proteins (Fig. 4a). We also knocked-down MKK7, an upstream activator of Jnk, by transfecting cells with an MMK7 siRNA. As found with SP600125, knocking-down MMK7 attenuated ADR-induced activation of Jnk and release of c-Abl from 14-3-3 proteins (see Supplementary Information, Fig. S3a). Exogenous expression of MMK7, which activates Jnk, was associated with dissociation of c-Abl and 14-3-3

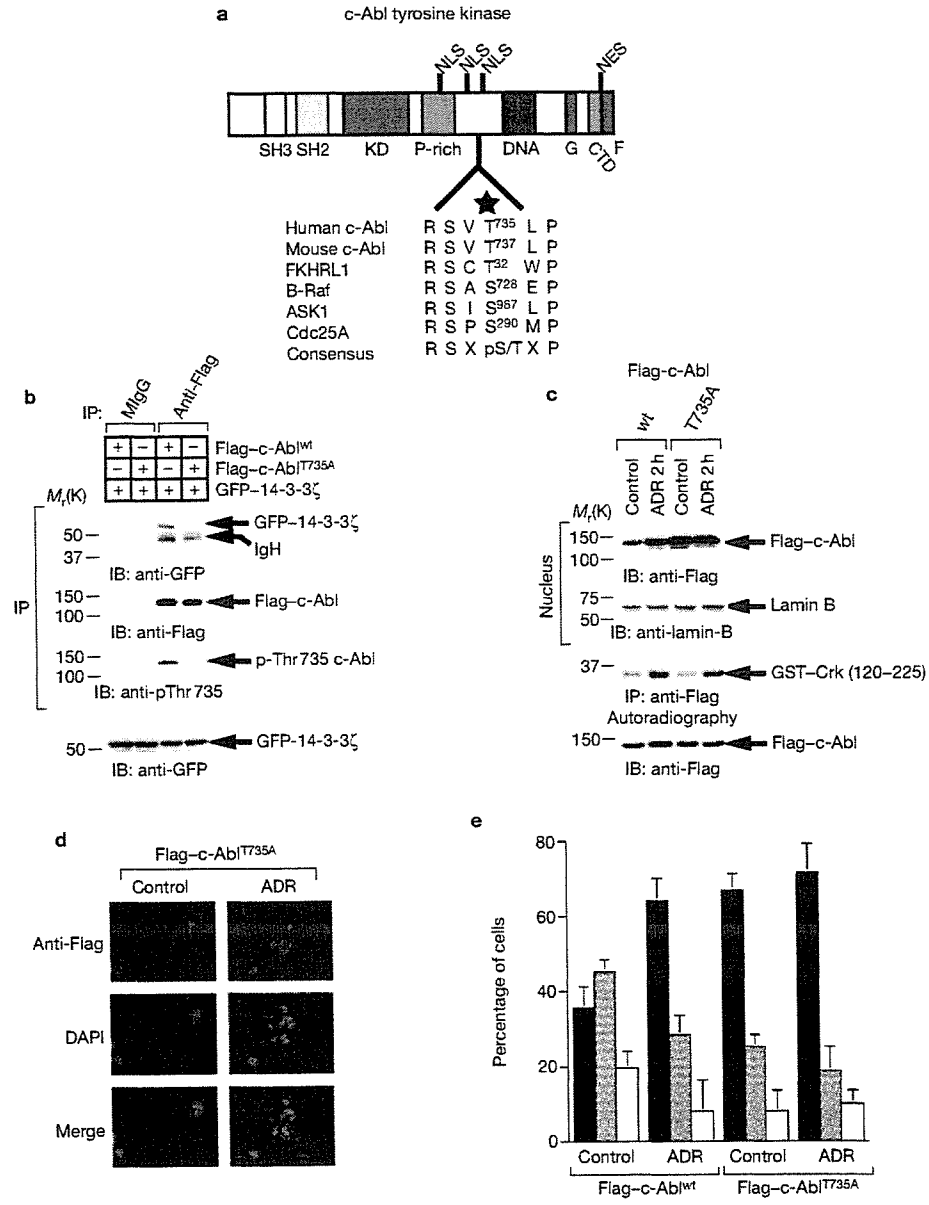

Figure 3 Phosphorylated Thr 735 of c-ABL is the binding site for 14-3-3 proteins. (**a**) Schematic representation of c-ABL tyrosine kinase. SH2, Src homology 2 domain; SH3, Src homology 3 domain; KD, catalytic tyrosine kinase domain; P-rich, proline-rich domain; DNA, DNA-binding domain; G, G-actin binding domain; CTD, RNA polymerase II carboxy-terminal domain binding region; F, F-actin binding domain; NLS, nuclear localization signal; NES, nuclear export signal. The sequence surrounding Thr 735 of c-ABL is shown in enlargement. Similar sequences from other 14-3-3 binding proteins and the consensus 14-3-3 binding motif are also listed. An asterisk marks the threonine/serine that is the putative phosphorylation and 14-3-3 binding site. (**b**) 293T cells were transfected with GFP-14-3-3ζ and Flag-c-ABL wild-type (wt) or T735A variant. Lysates were subjected to immunoprecipitation (IP) with normal mouse immunoglobulin G (MIgG) or anti-Flag, followed by immunoblotting (IB) with the indicated antibodies. Cell lysates were also subjected to immunoblot analysis with anti-GFP (bottom panel). (**c**) 293T cells transfected with Flag-c-ABL wt or T735A mutant were treated with adriamycin (ADR) for 2 h. Nuclear lysates were analysed by immunoblotting with anti-Flag (top panel) or anti-lamin-B (second panel). Anti-Flag immunoprecipitates from whole-cell lysates were incubated with GST-Crk(120-225) and analysed by autoradiography (third panel). Cell lysates were also subjected to immunoblot analysis with anti-Flag (bottom panel). (**d**) 293T cells were transfected with Flag-c-ABL T735A mutant and left untreated or were treated with ADR for 2 h. Fixed cells were stained with anti-Flag and DAPI (4',6-diamidino-2-phenylindole). (**e**) Quantitation of the results in Figs 1d and 3d. The localization of Flag-c-ABL was scored according to whether it was higher in the nucleus (closed bar), evenly distributed between the nucleus and the cytoplasm (dotted bar) or higher in the cytoplasm (open bar). Results are the mean ±SD of values obtained from five fields of 30–100 cells in each of three independent experiments.

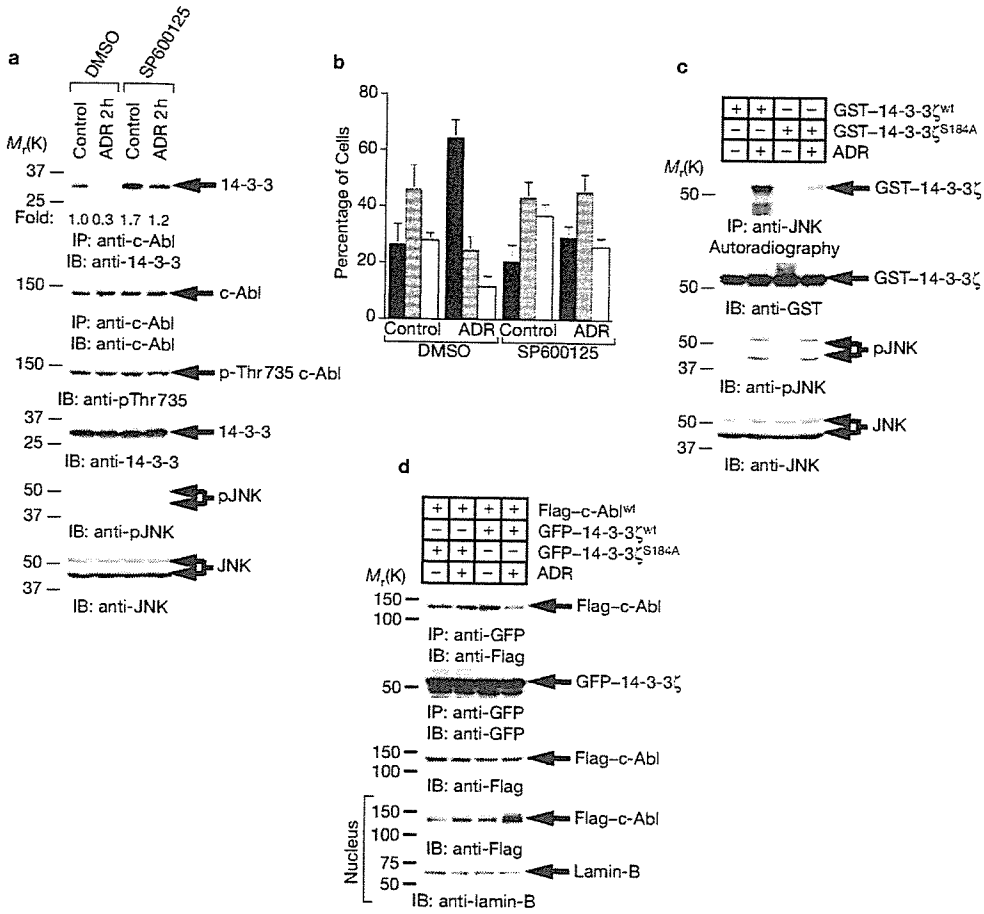

Figure 4 c-Jun N-terminal kinase (JNK) induces release of c-ABL from 14-3-3 proteins in response to DNA damage. (**a**) HeLa cells were treated with dimethyl sulphoxide (DMSO) or SP600125 for 30 min, followed by treatment with adriamycin (ADR). Cell lysates were subjected to immunoprecipitation (IP) with anti-c-ABL and immunoblot (IB) analysis with anti-14-3-3 (top panel) or anti-c-ABL (second panel). Lysates were also analysed by immunoblotting with anti-phospho-c-ABL (Thr 735) (anti-pThr^{735}; third panel), anti-14-3-3 (fourth panel), anti-phospho-JNK (anti-pJNK; fifth panel) or anti-JNK (bottom panel). Protein levels of immunoprecipitated 14-3-3 proteins were quantitated by comparison with the level in control cells. Fold induction was caluculated by comparing to the level in control cells. The results are expressed as the mean (standard error, <10%) of three independent experiments. (**b**) HeLa cells were treated as in **a**. Localization of c-ABL was quantitated as described in the legends to Fig. 3e. (**c**) HeLa cells were left untreated or were treated with ADR for 2 h. Anti-JNK-immunoprecipitates were incubated with glutathione *S*-transferase (GST)-14-3-3ζ wild type (wt) or S184A mutant and [γ-^{32}P]ATP for 15 min at 30 °C. Immunoprecipitation reaction products were resolved by SDS-PAGE and analysed by autoradiography (top panel) or by immunoblotting (IB) with anti-GST (second panel). Cell lysates were subjected to immunoblot analysis with anti-phospho-JNK (anti-pJNK; third panel) or anti-JNK (bottom panel). (**d**) 293T cells were transfected with Flag-c-ABL and GFP-14-3-3ζ wt or S184A mutant. After treatment with ADR for 2 h, whole-cell lysates were subjected to immunoprecipitation (IP) with anti-GFP. The immunoprecipitates were then analysed by immunoblotting with anti-Flag (top panel) or anti-GFP (second panel). Lysates were also subjected to immunoblot analysis with anti-c-ABL (third panel). Nuclear lysates were prepared and analysed by immunoblotting with anti-Flag (fourth panel) or with anti-lamin-B (bottom panel).

proteins (see Supplementary Information, Fig. S3c). Moreover, expression of a dominant-negative MMK7 blocked Jnk activation and release of c-Abl from 14-3-3 proteins (see Supplementary Information, Fig. S3c). It was also shown that downregulation of Jnk attenuated nuclear accumulation of c-Abl following DNA damage (Fig. 4b; also see Supplementary Information, Fig. S3b). To determine whether Jnk phosphorylation of 14-3-3 proteins on Ser 184 releases c-Abl, anti-Jnk immunoprecipitates from cells exposed to ADR were analysed for phosphorylation of 14-3-3ζ or a mutant in which Ser 184 was replaced with Ala (14-3-3ζ^{S184A}). ADR treatment was associated with Jnk phosphorylation of 14-3-3ζ and this response was decreased with the 14-3-3ζ^{S184A} mutant (Fig. 4c). ADR treatment was also associated with dissociation of c-Abl from wild-type 14-3-3ζ and not the 14-3-3ζ^{S184A} mutant (Fig. 4d). Similar findings were obtained in the treatment of cells with hydrogen peroxide (see Supplementary Information, Fig. S3d). These findings support a model in which Jnk phosphorylation of 14-3-3 proteins induces dissociation of the c-Abl 14-3-3 complex and thereby targeting of c-Abl to the nucleus.

To assess the functional significance of the interaction between c-Abl and 14-3-3 proteins, we examined the involvement of 14-3-3 in c-Abl-induced apoptosis. As shown previously[4], expression of c-Abl was associated with induction of apoptosis (Fig. 5a). Moreover, the apoptotic activity of c-Abl was enhanced by ADR treatment (Fig. 5a). By contrast, 14-3-3ζ attenuated c-Abl- and ADR-induced apoptosis

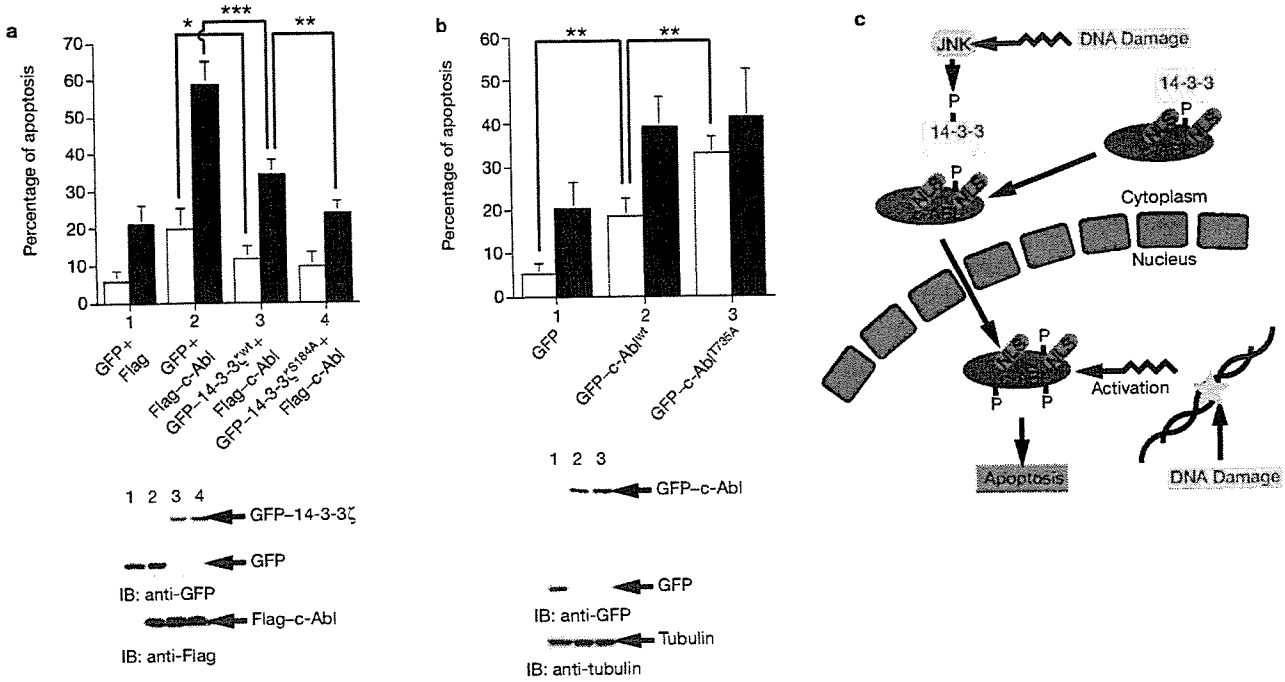

Figure 5 14-3-3 proteins attenuate c-ABL-mediated apoptosis in response to DNA damage. (**a**) 293T cells were transfected with Flag-c-ABL and green fluorescent protein (GFP) vector, GFP–14-3-3ζ wt or S184A mutant. At 24 h post-transfection, cells were left untreated or were treated with adriamycin (ADR) for 24 h. DNA content in cells that were positive for GFP was analysed by FACscan. The results (mean ±SD of eight independent experiments) are represented as the percentage of apoptotic cells with sub-G1 DNA ($*P<0.05$, $**P<0.01$ and $***P<0.005$). Control cells (open bars); ADR-treated cells (closed bars). Cells were also lysed and analysed by immunoblotting (IB) with anti-GFP (right, upper panel) or anti-Flag (right, lower panel). (**b**) *c-Abl*$^{-/-}$ murine embryonic fibroblasts were transfected with GFP vector, GFP-c-ABL or GFP-c-ABL^{T735A}. At 24 h post-transfection, cells were left untreated or treated with ADR for 24 h. DNA content in cells that were positive for GFP was analysed by FACscan. The results (mean ±SD of three independent experiments) are represented as the percentage of apoptotic cells with sub-G1 DNA ($**P<0.01$). Control cells (open bars); ADR-treated cells (closed bars). Cells were also lysed and analysed by immunoblotting with anti-GFP (right, upper panel) or anti-tubulin (right, lower panel). (**c**) A proposed model of the mechanism by which c-ABL translocates to the nucleus in response to DNA damage. Following DNA damage, cytoplasmic sequestration of c-ABL by 14-3-3 proteins is abrogated by c-Jun N-terminal kinase (JNK)-mediated 14-3-3 phosphorylation. Released c-ABL from 14-3-3 proteins then translocates to the nucleus. In the nucleus, c-ABL is activated by DNA damage and induces apoptosis. NLS, nuclear localization signal.

(Fig. 5a). Similar results were obtained in the apoptotic responses to etoposide and ara-C (data not shown). Attenuation of apoptosis was comparable when overexpressing wild-type 14-3-3ζ or the 14-3-3ζ^{S184A} mutant (Fig. 5a); however, following ADR exposure, expression of the 14-3-3ζ^{S184A} mutant conferred a more protective effect on c-Abl-mediated apoptosis (Fig. 5a). Similar results were obtained in the apoptotic response to oxidative stress (see Supplementary Information, Fig. S4a). To determine whether nuclear targeting of c-Abl is associated with induction of apoptosis, we fused various mutants of c-Abl with GFP (see Supplementary Information, Fig. S4b). As previously shown[1,2], the c-Abl NLS deletion mutant (c-AblΔNLS) or NES deletion mutant (c-AblΔNES) localized exclusively in the cytoplasm or the nucleus, respectively (see Supplementary Information, Fig. S4c). Similar patterns of localization were obtained when analysing the cells by fluorescence microscopy (data not shown). Expression of either GFP–c-Abl^{T735A} or GFP–c-AblΔNES was more effective than expression of wild-type c-Abl in inducing apoptosis (see Supplementary Information, Fig. S4d). By contrast, expression of GFP–c-AblΔNLS had little, if any, effect on the induction of apoptosis. Moreover, co-expression of 14-3-3ζ attenuated c-Abl-, but not c-Abl^{T735A}- or c-AblΔNES-induced apoptosis (see Supplementary Information, Fig. S4d). These results support a role for 14-3-3 proteins in inhibiting c-Abl-mediated apoptosis by sequestering c-Abl into the cytoplasm. To directly examine the involvement of 14-3-3 proteins in c-Abl-induced apoptosis, *c-Abl*$^{-/-}$ murine embryonic fibroblasts were transfected with GFP vector, GFP–c-Abl or GFP–c-Abl^{T735A}. Expression of GFP–c-Abl was associated with induction of apoptosis and this effect was enhanced by treatment of cells with ADR (Fig. 5b). Importantly, GFP–c-Abl^{T735A} was more effective than GFP–c-Abl in inducing apoptosis; however, the apoptotic effects of c-Abl and c-Abl^{T735A} were similar when c-Abl was treated with ADR (Fig. 5b). These findings provide support for the involvement of 14-3-3 proteins as negative regulators of apoptosis by cytoplasmic sequestration of c-Abl (Fig. 5c).

The seven isoforms of 14-3-3 have been implicated in regulating apoptosis by sequestering pro-apoptotic proteins, such as BAD, FKHRL1, ASK1, NUR77 and BAX[17–20]. Phosphorylation of the RSXpS/TXP motif on certain 14-3-3 binding proteins is necessary for the interaction with 14-3-3 proteins[21,22]. Other proteins, such as BAX, associate with 14-3-3 proteins by phosphorylation-independent mechanisms[23]. The present results demonstrate that c-Abl binds to 14-3-3 proteins and that this interaction is dependent on phosphorylation of c-Abl on Thr 735 in a conserved RSVTLP motif. Previous work has indicated that 14-3-3 proteins inhibit nuclear import of target proteins by interfering with NLS sites[16]. In this regard, the c-Abl RSVTLP motif resides between the second and third NLSs that are located at amino acids 707–720

and 759–772, respectively (Fig. 3a). The first c-Abl NLS at amino acids 601–615 could also be affected by binding of c-Abl to 14-3-3 proteins. Our results also indicate that Thr 735 phosphorylation is constitutive and not regulated by exposure to DNA-damaging agents. The kinase that is responsible for phosphorylation of c-Abl on Thr 735 is, at present, not known. Importantly, however, expression of c-Abl with a T735A mutation disrupted binding to 14-3-3 proteins and resulted in targeting of c-Abl to the nucleus. These findings indicate that nuclear import of c-Abl is regulated by binding to 14-3-3 proteins in the cytoplasm.

Post-translational modifications of 14-3-3 proteins have been shown to modulate their binding affinity to target proteins[24]. Moreover, recent work has shown that Jnk-mediated phosphorylation of 14-3-3 proteins induces their release from BAX[17]. The present studies demonstrate that Jnk phosphorylation of 14-3-3 proteins induces their release from c-Abl. Jnk has been shown to phosphorylate 14-3-3ζ on Ser 184 (ref. 17). In this context, expression of a Jnk phosphorylation site 14-3-3ζ^{S184A} mutant attenuated DNA-damage-induced localization of c-Abl in the nucleus. These findings collectively support a model in which Jnk phosphorylates 14-3-3 proteins and releases cytoplasmic pools of c-Abl for import into the nucleus and thereby amplification of the apoptotic response (Fig. 5c). Together with this model, the c-Abl kinase function was dispensible for release of c-Abl from 14-3-3 proteins and for import of c-Abl into the nucleus. Previous studies show that, following apoptotic stimuli, 14-3-3 proteins are cleaved by caspases at the C-terminal region, resulting in release of BAD or BAX to the mitochondrial membrane[23,25]. Although this model represents another potential mechanism for dissociation of c-Abl from 14-3-3 proteins, only two isomers of 14-3-3 — ε and θ — are reported to be caspase substrates[23,25]. Moreover, caspase activation occurs in relatively later periods following DNA damage. Given the present findings that nuclear targeting of c-Abl is prompt and transient, it is conceivable that Jnk phosphorylation of 14-3-3 proteins is an initial step for the release of c-Abl. Our results also show that expression of the 14-3-3ζ^{S184A} mutant attenuates c-Abl-mediated apoptosis in the DNA-damage response. Sequestration of c-Abl into the cytoplasm by binding to 14-3-3 proteins therefore represents a potential mechanism by which cells modulate the apoptotic response to genotoxic stress.

METHODS

Cell culture. Human HeLa, 293T embryonal kidney and MCF-7 breast carcinoma cells (ATCC) and murine embryonic fibroblasts[10] were cultured in Dulbecco's modified Eagle's medium (DMEM) supplemented with 10% heat-inactivated fetal bovine serum (FBS), 100 units/ml penicillin, 100 μg ml^{-1} streptomycin and 2 mM L-glutamine. Human U-937 and HL-60 myeloid leukaemia cells (ATCC) were grown in RPMI 1640 medium containing 10% FBS, antibiotics and L-glutamine. Cells were treated with 1 μM ADR (Sigma-Aldrich, St Louis, MO), 10 μM etoposide (Sigma-Aldrich), 10 μM ara-C (Sigma-Aldrich), hydrogen peroxide (Nakalai Tesque, Kyoto, Japan) or 10 μM SP600125 (Calbiochem-Novabiochem, San Diego, CA).

Plasmids. 14-3-3ζ and 14-3-3σ cDNAs were isolated by reverse transcription PCR (RT-PCR) from HeLa cells and cloned into pGFP-C1 (BD Clontech, Palo Alto, CA) and pGEX4T1 (Amersham Biosciences, Piscataway, NJ). Site-directed mutagenesis was performed and the mutation was confirmed by DNA sequencing. c-Abl wild-type and c-Abl (K-R) cDNAs were prepared as described elsewhere[4]. Glutathione *S*-transferase (GST)-tagged Jnk and MKK7 were also prepared as described previously[26].

Cell transfections. Cell transfections were performed as described previously[4,10]. The total DNA concentration was kept constant by including an empty vector.

Protein identification by LC-MS/MS analysis. Flag-c-Abl-associated complexes were digested with Lys-C, and the resulting peptides were analysed using a nanoscale liquid chromatography-mass spectrometry (MS)/MS system as described previously[14].

Immunoprecipitation and immunoblot analysis. Cell lysates were prepared[27] and cleared by centrifugation at 12,000 *g* for 15 min. Soluble proteins were incubated with anti-Flag (Sigma-Aldrich), anti-GFP (Nakalai Tesque), anti-c-Abl (Santa Cruz Biotechnology, Santa Cruz, CA), anti-14-3-3 protein (Upstate, Charlottesville, VA) or anti-Jnk (Santa Cruz Biotechnology) antibodies for 2 h at 4 °C followed by a 1 h incubation with protein A- (Amersham Biosciences) or G- (Zymed Laboratories, South San Francisco, CA) Sepharose beads. The immune complexes were washed three times with lysis buffer. Cell lysates or immunoprecipitates were separated by SDS-PAGE and transferred to nitrocellulose filters. The filters were then incubated with anti-Flag, anti-GFP, anti-c-Abl (Calbiochem-Novabiochem), anti-phospho-c-Abl (Thr 735) (Cell Signaling Technology, Beverly, MA), anti-14-3-3 (Santa Cruz Biotechnology), anti-Jnk, anti-phospho-Jnk (Cell Signaling Technology), anti-MKK7 (Santa Cruz Biotechnology), anti-GST (Nakalai Tesque) or anti-tubulin (Sigma-Aldrich). The antigen–antibody complexes were visualized using chemiluminescence (PerkinElmer, Wellesley, MA).

Subcellular fractionation. Subcellular fractionation was performed as described previously[7]. Purity of the fractions was monitored by immunoblot analysis with anti-lamin-B (Calbiochem-Novabiochem) and anti-IκBα (Santa Cruz Biotechnology).

Immunofluorescence assays. Cells were cultured in 4-well chamber slides. After washing once with phosphate-buffered saline (PBS), cells were fixed in 3.2% paraformaldehyde and permeabilized in 0.5% Triton X-100 in PBS for 10 min. Fixed cells were washed twice in PBS and blocked with 5% goat serum in PBS for 1 h. After washing with PBS three times, cells were incubated with anti-Flag, anti-c-Abl (BD PharMingen, San Diego, CA) or anti-14-3-3 protein for 3 h. Immune complexes were then stained with goat anti-mouse immunoglobulin G conjugated with fluorescein (FITC) or rhodamine (TRITC) antibodies (Sigma-Aldrich). Stained cells were mounted with Vectashield Mounting Medium with 4′,6-diamidino-2-phenylindole (DAPI; Vector Laboratories, Burlingame, CA) and analysed with a Nikon Eclipse TE2000-U microscope.

siRNA transfections. Small interfering RNAs (siRNAs) were synthesized and purified by Qiagen (Valencia, CA). The siRNA sequence for targeting MKK7 was described elsewhere[25]. GFP siRNA were used as a negative control[27]. 14-3-3 protein siRNAs were purchased from Santa Cruz Biotechnology. Transfection of siRNAs was performed in the presence of oligofectamine (Invitrogen, Carlsbad, CA).

***In vitro* kinase assays.** *In vitro* kinase assays were performed as described previously, using GST-Crk(120-225) or GST-14-3-3ζ as a substrate[26].

Assessment of apoptosis. DNA content was assessed by staining ethanol-fixed cells with propidium iodide and monitoring by FACScan (Becton Dickinson, San Jose, CA). The numbers of cells that were positive for green fluorescence with sub-G_1 DNA content were determined using the CellQuest program (Becton Dickinson).

BIND identifiers. Four BIND identifiers (www.bind.ca) are associated with this manuscript: 199701, 199702, 199703 and 199704.

Note: Supplementary Information is available on the Nature Cell Biology website.

ACKNOWLEDGEMENTS

This work was supported by grants from the Ministry of Education, Science and Culture of Japan (K.Y. and Y.M.), the Mitsubishi Pharma Research Foundation (K.Y.), the Tokyo Biochemical Research Foundation (K.Y.), Uehara Memorial Foundation (K.Y.) and also by grants CA29431 and CA98628 from the National Cancer Institute (D.K.).

COMPETING FINANCIAL INTERESTS

The authors declare that they have no competing financial interests.

Received 10 November 2004; accepted 17 December 2004
Published online at http://www.nature.com/naturecellbiology.

1. Wen, S. T., Jackson, P. K. & Van Etten, R. A. The cytostatic function of c-Abl is controlled by multiple nuclear localization signals and requires the p53 and Rb tumor suppressor gene products. *EMBO J.* **15**, 1583–1595 (1996).
2. Taagepera, S. *et al.* Nuclear-cytoplasmic shuttling of c-ABL tyrosine kinase. *Proc. Natl Acad. Sci. USA* **95**, 7457–7462 (1998).
3. Kharbanda, S. *et al.* Activation of the c-Abl tyrosine kinase in the stress response to DNA-damaging agents. *Nature* **376**, 785–788 (1995).
4. Yuan, Z. M. *et al.* Regulation of DNA damage-induced apoptosis by the c-Abl tyrosine kinase. *Proc. Natl Acad. Sci. USA* **94**, 1437–1440 (1997).
5. Wetzler, M. *et al.* Subcellular localization of Bcr, Abl, and Bcr-Abl proteins in normal and leukemic cells and correlation of expression with myeloid differentiation. *J. Clin. Invest.* **92**, 1925–1939 (1993).
6. Raitano, A. B., Whang, Y. E. & Sawyers, C. L. Signal transduction by wild-type and leukemogenic Abl proteins. *Biochim. Biophys. Acta* **1333**, F201–F216 (1997).
7. Vigneri, P. & Wang, J. Y. Induction of apoptosis in chronic myelogenous leukemia cells through nuclear entrapment of BCR–ABL tyrosine kinase. *Nature Med.* **7**, 228–234 (2001).
8. Sun, X., Wu, F., Datta, R., Kharbanda, S. & Kufe, D. Interaction between protein kinase C delta and the c-Abl tyrosine kinase in the cellular response to oxidative stress. *J. Biol. Chem.* **275**, 7470–7473 (2000).
9. Druker, B. J. *et al.* Effects of a selective inhibitor of the Abl tyrosine kinase on the growth of Bcr–Abl positive cells. *Nature Med.* **2**, 561–566 (1996).
10. Yoshida, K., Komatsu, K., Wang, H. G. & Kufe, D. c-Abl tyrosine kinase regulates the human Rad9 checkpoint protein in response to DNA damage. *Mol. Cell. Biol.* **22**, 3292–3300 (2002).
11. Gong, J. G. *et al.* The tyrosine kinase c-Abl regulates p73 in apoptotic response to cisplatin-induced DNA damage. *Nature* **399**, 806–809 (1999).
12. Agami, R., Blandino, G., Oren, M. & Shaul, Y. Interaction of c-Abl and p73α and their collaboration to induce apoptosis. *Nature* **399**, 809–813 (1999).
13. Yuan, Z. M. *et al.* p73 is regulated by tyrosine kinase c-Abl in the apoptotic response to DNA damage. *Nature* **399**, 814–817 (1999).
14. Natsume, T. *et al.* A direct nanoflow liquid chromatography-tandem mass spectrometry system for interaction proteomics. *Anal. Chem.* **74**, 4725–4733 (2002).
15. Tzivion, G. & Avruch, J. 14-3-3 proteins: active cofactors in cellular regulation by serine/threonine phosphorylation. *J. Biol. Chem.* **277**, 3061–3064 (2002).
16. Muslin, A. J. & Xing, H. 14-3-3 proteins: regulation of subcellular localization by molecular interference. *Cell Signal.* **12**, 703–709 (2000).
17. Tsuruta, F. *et al.* JNK promotes Bax translocation to mitochondria through phosphorylation of 14-3-3 proteins. *EMBO J.* **23**, 1889–1899 (2004).
18. Zha, J., Harada, H., Yang, E., Jockel, J. & Korsmeyer, S. J. Serine phosphorylation of death agonist BAD in response to survival factor results in binding to 14-3-3 not BCL-X(L). *Cell* **87**, 619–628 (1996).
19. Zhang, L., Chen, J. & Fu, H. Suppression of apoptosis signal-regulating kinase 1-induced cell death by 14-3-3 proteins. *Proc. Natl Acad. Sci. USA* **96**, 8511–8515 (1999).
20. Masuyama, N. *et al.* Akt inhibits the orphan nuclear receptor Nur77 and T-cell apoptosis. *J. Biol. Chem.* **276**, 32799–32805 (2001).
21. Muslin, A. J., Tanner, J. W., Allen, P. M. & Shaw, A. S. Interaction of 14-3-3 with signaling proteins is mediated by the recognition of phosphoserine. *Cell* **84**, 889–897 (1996).
22. Yaffe, M. B. *et al.* The structural basis for 14-3-3:phosphopeptide binding specificity. *Cell* **91**, 961–971 (1997).
23. Nomura, M. *et al.* 14-3-3 interacts directly with and negatively regulates pro-apoptotic Bax. *J. Biol. Chem.* **278**, 2058–2065 (2003).
24. Aitken, A. *et al.* Specificity of 14-3-3 isoform dimer interactions and phosphorylation. *Biochem. Soc. Trans.* **30**, 351–360 (2002).
25. Won, J. *et al.* Cleavage of 14-3-3 protein by caspase-3 facilitates bad interaction with Bcl-x(L) during apoptosis. *J. Biol. Chem.* **278**, 19347–19351 (2003).
26. Yoshida, K., Weichselbaum, R., Kharbanda, S. & Kufe, D. Role for Lyn tyrosine kinase as a regulator of stress-activated protein kinase activity in response to DNA damage. *Mol. Cell. Biol.* **20**, 5370–5380 (2000).
27. Yoshida, K., Wang, H. G., Miki, Y. & Kufe, D. Protein kinase Cδ is responsible for constitutive and DNA damage-induced phosphorylation of Rad9. *EMBO J.* **22**, 1431–1441 (2003).
28. Deng, Y., Ren, X., Yang, L., Lin, Y. & Wu, X. A JNK-dependent pathway is required for TNFα-induced apoptosis. *Cell* **115**, 61–70 (2003).

nature
cell biology

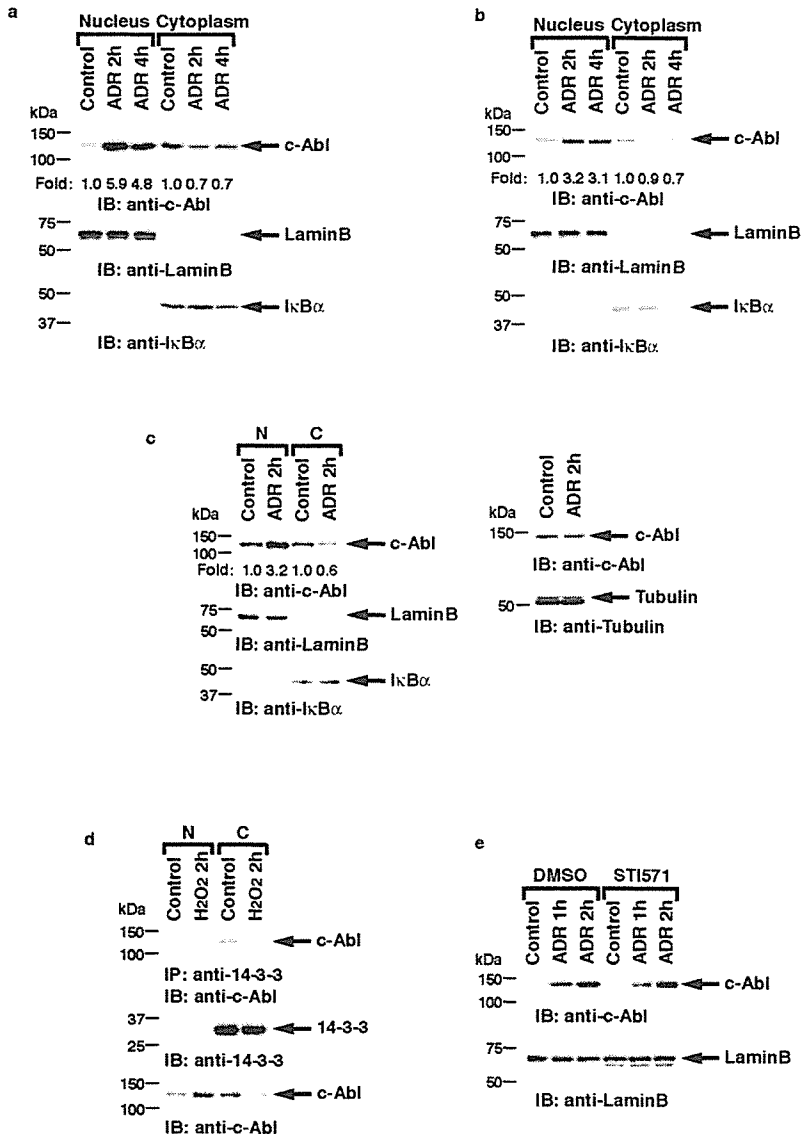

Figure S1 c-Abl translocates to the nucleus following DNA damage or oxidative stress in various cell types. (a-c) HL-60 (a), MCF-7 (b) and U-937 (c) cells were left untreated or treated with ADR for the indicated times. Nuclear and cytoplasmic lysates were analyzed by immunoblotting with anti-c-Abl (upper panel), anti-LaminB (middle panel) or anti-IκBα (lower panel). Whole cell lysates from U-937 cells were subjected to immunoblot analysis with anti-c-Abl (right, upper panel) or anti-Tubulin (right, lower panel). (d) U-937 cells were treated with 50 μM hydrogen peroxide (H_2O_2) for 2 h. Nuclear and cytoplasmic lysates were subjected to immunoprecipitation with anti-14-3-3 and then immunoblot analysis with anti-c-Abl (upper panel). Lysates were also analyzed by immunoblotting with anti-14-3-3 (middle panel) or anti-c-Abl (lower panel). (e) Kinase activity is dispensible for nuclear targeting of c-Abl in response to DNA damage. HeLa cells were treated with DMSO or 10 μM STI571 for 30 min followed by treatment with ADR. Cell lysates were subjected to immunoblot analysis with anti-c-Abl (upper panel) or anti-LaminB (lower panel).

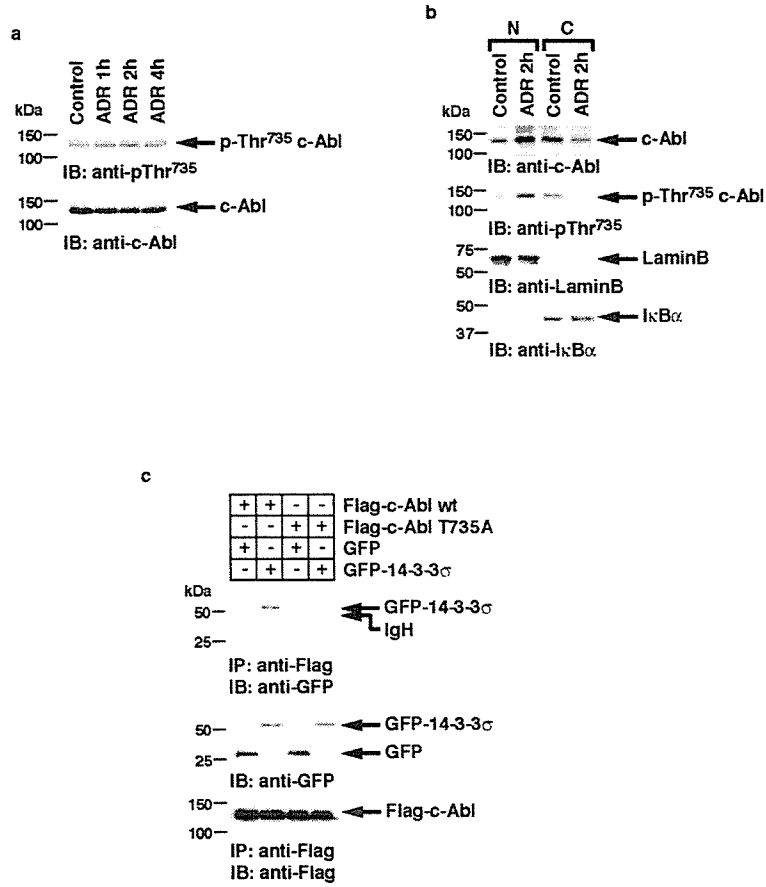

Figure S2 Thr735 in c-Abl is the major binding target for 14-3-3. (a) HeLa cells were left untreated or treated with ADR for the indicated times. Cell lyates were subjected to immunoblot analysis with anti-phospho-c-Abl (Thr735) (upper panel) or anti-c-Abl (lower panel). (b) HeLa cells were left untreated or treated with ADR for 2h. Cell lysates from nuclear and cytoplasmic fractions were analyzed by immunoblotting with indicated antibodies. (c) 293T cells were transfected with Flag-c-Abl, Flag-c-Abl(T735A), GFP-vector or GFP-14-3-3σ. Cell lysates were immunoprecipitated with anti-Flag. The immunoprecipitates were subjected to immunoblot analysis with anti-GFP (upper panel) or anti-Flag (lower panel). Lysates were also analyzed by immunoblotting with anti-GFP (middle panel).

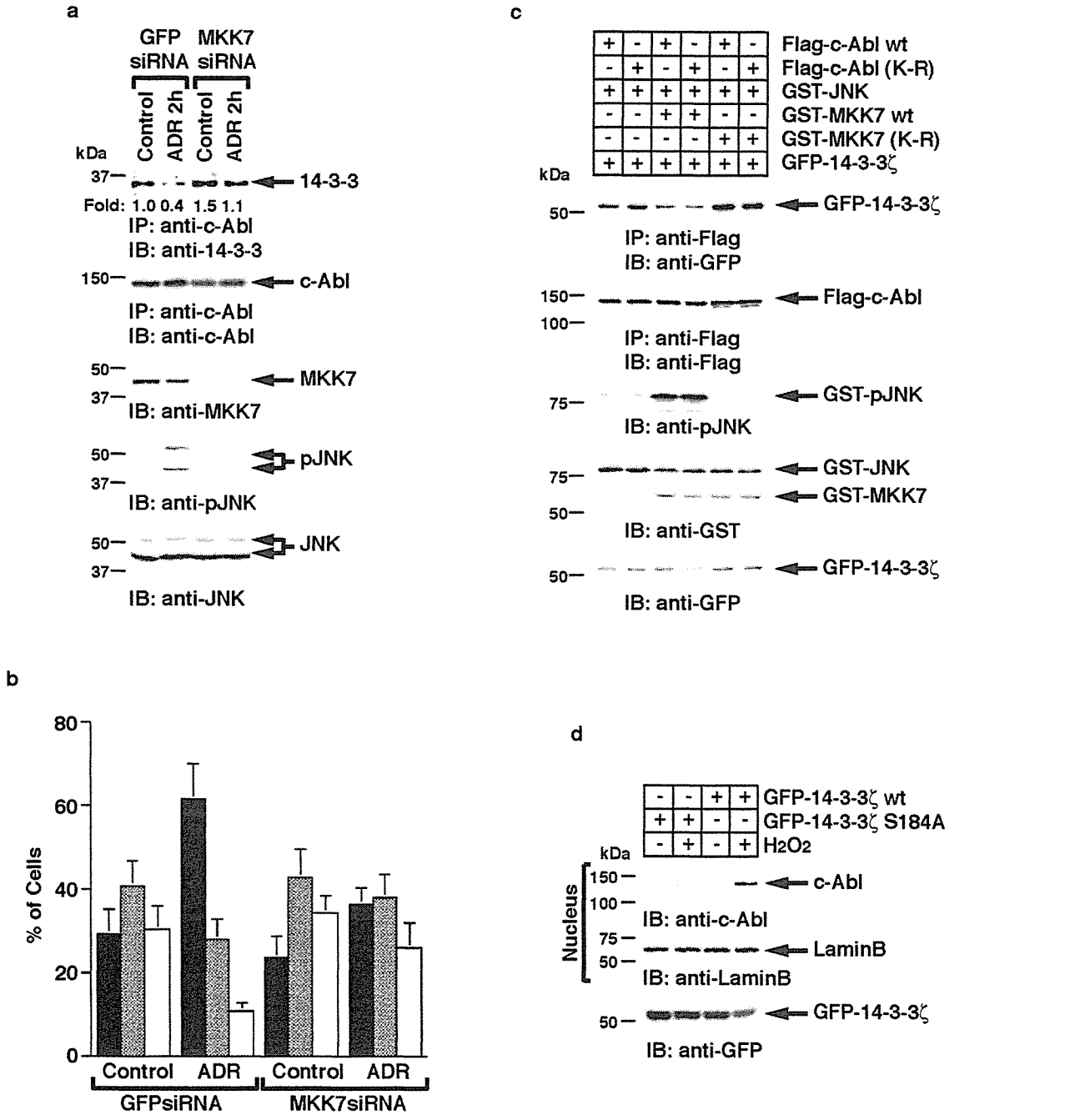

Figure S3 c-Abl-14-3-3 complexes are disrupted by activation of JNK. (a) HeLa cells were transfected with GFPsiRNA or MKK7siRNA. Cell lysates were subjected to immunoprecipitation with anti-c-Abl. The immunoprecipitates were analyzed by immunoblotting with anti-14-3-3 (top panel) or anti c-Abl (second panel). Lysates were also subjected to immunoblot analysis with anti-MKK7 (third panel), anti-phospho-JNK (fourth panel) or anti-JNK (bottom panel) (b) HeLa cells were treated as in (a). Localization of c-Abl was quantitated as described in the legends to Fig. 3e. (c) 293T cells were transfected as indicated. After 48 h post-transfection, cell lysates were immunoprecipitated with anti-Flag. The immunoprecipitates were then subjected to immunoblot analysis with anti-GFP (top panel) or anti-Flag (second panel). Lysates were also analyzed by immunoblotting with anti-GST (third panel) or anti-GFP (bottom panel). (d) 293T cells were transfected with GFP-14-3-3ζ wt or the S184A mutant. After treatment with 50 μM H_2O_2 for 2 h, nuclear lysates were prepared and analyzed by immunoblotting with anti-c-Abl (upper panel) or anti-LaminB (middle panel). Whole cell lysates were subjected to immunoblot analysis with anti-GFP (lower panel).

STAT3 regulates Nemo-like kinase by mediating its interaction with IL-6-stimulated TGFβ-activated kinase 1 for STAT3 Ser-727 phosphorylation

Hirotada Kojima*, Takanori Sasaki*, Tohru Ishitani†, Shun-ichiro Iemura‡, Hong Zhao*, Shuhei Kaneko*, Hiroyuki Kunimoto*, Tohru Natsume‡, Kunihiro Matsumoto†, and Koichi Nakajima*§

*Department of Immunology, Osaka City University Graduate School of Medicine, 1-4-3 Asahi-machi, Abeno-ku, Osaka 545-8585, Japan; †Department of Molecular Biology, Graduate School of Science, Nagoya University, Chigusa-ku, Nagoya 464-8603, Japan; and ‡National Institutes of Advanced Industrial Science and Technology, Biological Information Research Center, Kohtoh-ku, Tokyo 135-0064, Japan

Communicated by Tadamitsu Kishimoto, Osaka University, Osaka, Japan, January 26, 2005 (received for review November 24, 2004)

Signal transducer and activator of transcription 3 (STAT3) is activated by the IL-6 family of cytokines and growth factors. STAT3 requires phosphorylation on Ser-727, in addition to tyrosine phosphorylation on Tyr-705, to be transcriptionally active. In IL-6 signaling, the two major pathways that derive from the YXXQ and the YSTV motifs of gp130 cause Ser-727 phosphorylation. Here, we show that TGF-β-activated kinase 1 (TAK1) interacts with STAT3, that the TAK1-Nemo-like kinase (NLK) pathway is efficiently activated by IL-6 through the YXXQ motif, and that this is the YXXQ-mediated H7-sensitive pathway that leads to STAT3 Ser-727 phosphorylation. Because NLK was recently shown to interact with STAT3, we explored the role of STAT3 in activating this pathway. Depletion of STAT3 diminished the IL-6-induced NLK activation by >80% without inhibiting IL-6-induced TAK1 activation or its nuclear entry. We found that STAT3 functioned as a scaffold for TAK1 and NLK *in vivo* through a region in its carboxyl terminus. Furthermore, the expression of the $STAT3_{534-770}$ region in the nuclei of STAT3-knockdown cells enhanced the IL-6-induced NLK activation in a dose-dependent manner but not the TGFβ-induced NLK activation. TGFβ did not cause STAT3 Ser-727 phosphorylation, even when the carboxyl region of STAT3 was expressed in the nuclei. Together, these results indicate that STAT3 enhances the efficiency of its own Ser-727 phosphorylation by acting as a scaffold for the TAK1-NLK kinases, specifically in the YXXQ motif-derived pathway.

gp130 | YXXQ motif | signaling specificity

The signal transducer and activator of transcription (STAT) family plays pivotal roles in a variety of systems and in development, in response to cytokines and growth factors. STAT family members are activated in the cytoplasm by tyrosine phosphorylation, form dimers, and enter the nucleus, where they act as DNA-binding transcription factors (1). Of the seven known STATs, STAT1, 3, 5A, 5B, and 6 are phosphorylated at one or two serine residues in their carboxyl-terminal transactivation domain (1, 2) and at a critical tyrosine. The serine phosphorylation enhances the transcriptional activity in the case of STAT1 (3), STAT3 (3, 4), and STAT6 (5). STAT3 can be activated by a variety of cytokines, including the IL-6 family, by using gp130 as a common receptor subunit (6). Granulocyte colony-stimulating factor (G-CSF) and erythropoietin, and growth factors, EGF, platelet-derived growth factor, and hepatocyte growth factor, and cytoplasmic tyrosine kinases, including Src and v-Eyk (reviewed in ref. 7). IL-6 uses STAT3 in its major signaling pathway and concomitantly activates the Ras/Raf/ERK and PI3-kinase pathways (7). IL-6, therefore, activates multiple genes, including acute-phase reactants, and the *junB*, *tis11*, *stat3*, c-*myc*, and c-*fos* genes, mostly through STAT3 (8–14). In the IL-6 receptor system, the tyrosine-phosphorylated YXXQ motif of gp130 is critical for recruiting STAT3 for subsequent phosphorylation at Tyr-705 by the associated Jak kinases (15). In addition, Abe *et al.* (4) showed that the YXXQ motif has another important role in activating STAT3, by phosphorylating Ser-727 through an H7-sensitive kinase pathway in response to IL-6, even at low concentrations. At higher concentrations of IL-6, another PD98059-sensitive pathway derived from the YSTV motif of gp130 also participates in STAT3 Ser-727 phosphorylation (4).

TGF-β-activated kinase 1 (TAK1) is a mitogen-activated protein MAP kinase kinase kinase that is activated by the TGFβ family, IL-1β, TNFα, and the Toll-like receptor family (16–19). TAK1 works with TAB1 (17), TAB2 (20), and TAB3 (21–23) to activate downstream kinases, including the IκB kinases, leading to NF-κB activation, and MAP kinase kinase (MKK) 3/6 and MKK4/7, leading, respectively, to p38 and JNK activation (16, 18, 24, 25). Recently, TAK1 was shown to activate Nemo-like kinase (NLK) in TGFβ (26), Wnt5a (27), and Wnt1 (28) signaling. More recently, Ohkawara *et al.* (29) showed that the TAK1-NLK pathway plays a critical role in TGFβ-induced mesodermal development in *Xenopus* embryos by phosphorylating STAT3 at Ser-727. However, it remains unclear how TAK1 and NLK select their downstream targets in the different signaling pathways.

In this study, we identified TAK1 in the STAT3 complex by using a combination of tandem affinity purification (TAP) and MS. We then found that TAK1 and its downstream kinase, NLK, were selectively activated by IL-6 through the YXXQ motif of gp130. We showed that TAK1 and NLK are critical components of the YXXQ-derived H7-sensitive kinase pathway leading to STAT3 Ser-727 phosphorylation. We further showed that STAT3 specifically enhances the IL-6-induced TAK1-dependent NLK activation, but not TGFβ-induced NLK activation, by acting as a specific scaffold for the kinases involved in the IL-6 signaling. Thus, the upstream TAK1, which is differentially activated by different signaling pathways, seems to select its specific downstream effector kinases in conjunction with a specific scaffold protein, which is STAT3 in the case of the IL-6 signal.

Methods

Cytokines, Abs, and Reagents. The recombinant human IL-6 and G-CSF were gifts from Ajinomoto (Kawasaki, Japan) and Kirin Brewery (Tokyo), respectively. All other cytokines were from PeproTech (London). Rabbit anti-STAT3 and anti-TAK1 Abs were described (18, 30). Anti-phospho-Ser-727 and phospho-Tyr-705 STAT3 Abs were from Cell Signaling Technology (Beverly, MA). Rabbit anti-GST Ab was from Upstate Biotech-

Abbreviations: STAT, signal transducer and activator of transcription; TAK1, TGF-β-activated kinase 1; NLK, Nemo-like kinase; RNAi, RNA interference; TAP, tandem affinity purification; G-CSF, granulocyte colony-stimulating factor; MAP, mitogen-activated protein; MKK, MAP kinase kinase; HA, hemagglutinin; WCE, whole-cell extract; LV, lentivirus.

§To whom correspondence should be addressed. E-mail: knakajima@med.osaka-cu.ac.jp.

www.pnas.org/cgi/doi/10.1073/pnas.0500679102

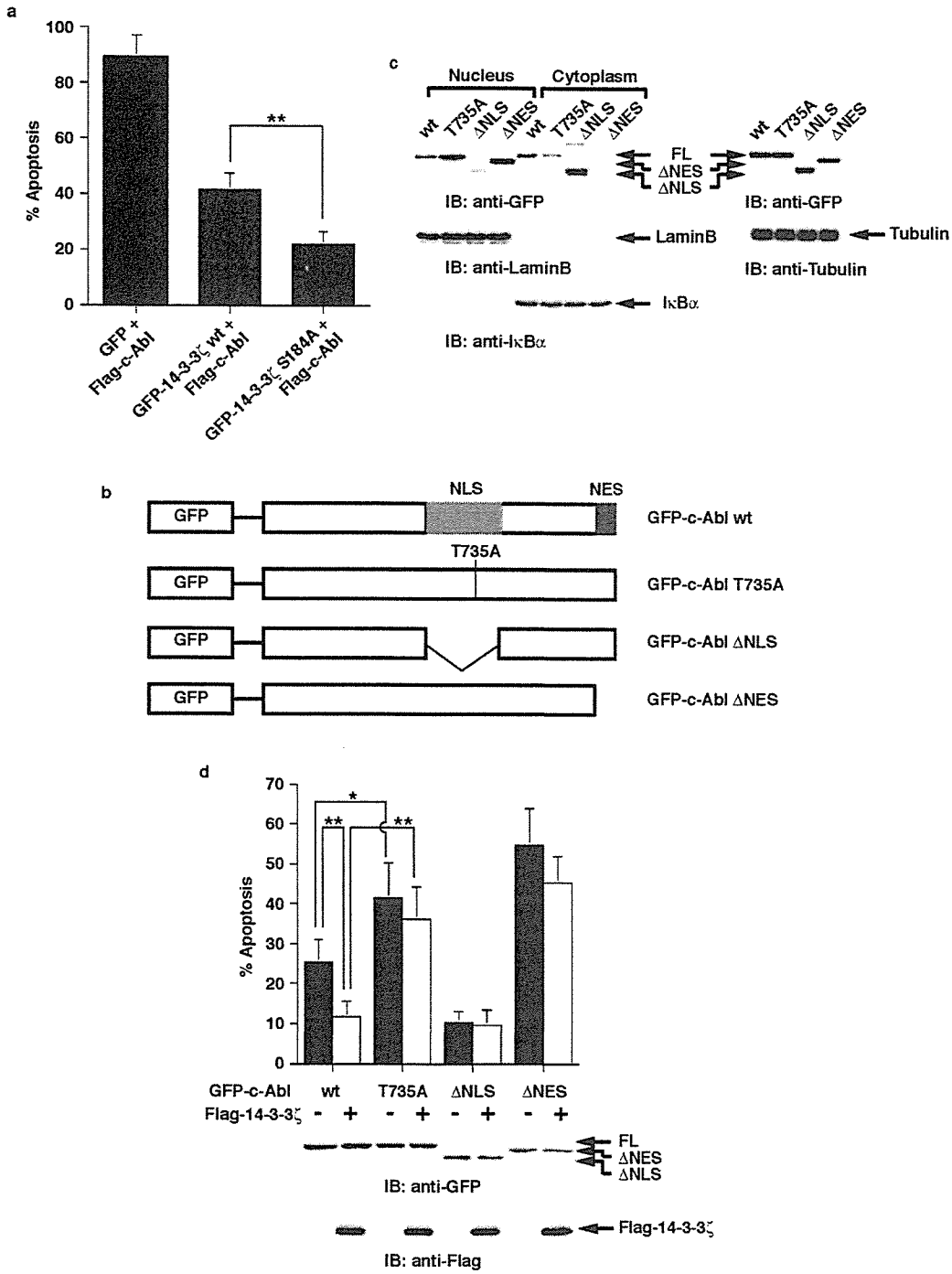

Figure S4 Nuclear targeting of c-Abl is required for the induction of apoptosis. (a) 293T cells were transfected with Flag-c-Abl and GFP vector, GFP-14-3-3ζ wt or S184A mutant. At 24 h post-transfection, cells were treated with 200 μM H_2O_2 for 8 h. DNA content in cells positive for green fluorescence was analyzed by FACscan. The results (mean ± S.D. of eight independent experiments) are represented as the percentage of apoptotic cells with sub-G1 DNA. (b) Constructs of GFP-fused c-Abl and the indicated mutants. (c) 293T cells were transfected with various GFP-c-Abl constructs shown in (b). Nuclear and cytoplasmic lysates were subjected to immunoblot analysis with anti-GFP (left, upper panel), anti-LaminB (left, middle panel) or anti-IκBα (left, lower panel). Whole cell lysates were analyzed by immunoblotting with anti-GFP (right, upper panel) or anti-Tubulin (right, lower panel). (d) 293T cells were co-transfected with the indicated GFP-c-Abl constructs in the presence and absence of Flag-14-3-3ζ. DNA content in cells positive for green fluorescence was analyzed by FACscan. The results (mean ± S.D. of three independent experiments) are represented as the percentage of apoptotic cells with sub-G1 DNA. Cell lysates were subjected to immunoblot analysis with anti-GFP (upper panel) or anti-Flag (lower panel).

nology (Lake Placid, NY). Anti-HA Mo Ab (12CA5) was from Boehringer Mannheim (Mannheim, Germany). All other Abs were from Santa Cruz Biotechnology. H7, 1-(5-iso-quinolinylsulfonyl)-2-methylpiperazine, and all other reagents were from Sigma-Aldrich (St. Louis).

Cell Lines. All of the cell lines were grown in DMEM supplemented with 10% FCS and the appropriate antibiotics. HepG2-G108YRHQ and HepG2-G108YSTV were described (4). The HepG2 cell line with knocked-down *stat3* mRNA (HepG2-STAT3KD) and its derivative cell line with RNA interference (RNAi)-resistant STAT3 (HepG2-KD-STAT3R) were described (14). For the kinase assays, HepG2 cells were cultured in DMEM containing 0.5% FCS for 36 h before stimulation.

Plasmids. The expression vectors encoding the hemagglutinin (HA)-STAT3 and HA-TAK1 were described (18, 31). The TAP tag was attached to the amino terminus of mouse STAT3 (ref. 32 and modified by K.N.), and the TAP-Stat3 cDNA was inserted into the pEF-BOS expression vector (a gift from S. Nagata, Osaka University, Osaka). pCMV-Myc-NLK was generated by inserting a PCR-generated cDNA encoding human NLK into pCDNAMyc (a gift from K. Iwai, Osaka City University, Osaka). For the lentivirus (LV)-mediated expression system, the Myc-NLK cDNA was subcloned into a pCSII-EF-MCS-IRES2-Venus vector (a gift from H. Miyoshi, RIKEN, Tsukuba, Japan). A cDNA fragment encoding $STAT3_{534-770}$ was made by PCR and fused to NLS-FLAG at the amino terminus, and the resultant cDNA was subcloned into the pCSII-EF-MCS-IRES2-Venus vector. All constructs were verified by DNA sequencing. pEF-GST and pEF-GST-$STAT3_{533-770}$ were described (4).

TAP and MS Analysis. TAP was performed as described (32). Briefly, TAP-STAT3 was stably expressed in 293T-G133 cells. Protein complexes interacting with STAT3 were then sequentially affinity-purified by using IgG-Sepharose, Tobacco etch virus protease digestion, and calmodulin beads. The eluates of calmodulin beads were digested with trypsin, and the resultant peptides were subjected to splitless nanoflow liquid chromatography coupled to nanoelectrospray tandem MS (33).

EMSA. ^{32}P-labeled oligonucleotides containing an NF-κB-binding site (5′-AGTGAGGGGACTTTCCGAGTG-3′) from the intercellular adhesion molecule-1 promoter and nuclear extracts from HepG2 cells were used.

LV-Mediated Expression of RNAi. We generated RNAi constructs in the plasmid pU6i-cassette (Genofunction) (34). The target positions of the RNAi against human TAK1 and human NLK were as follows: TAK1, GAGATCGACTACAAGGAGA; NLK, GGCGCACCATCATCAGCAC. To construct the lentiviral RNAi expression system, the cassette containing the U6 promoter and the RNAi was transferred into an LV vector, CS-RfA-EG, with the EF1α promoter-driven GFP gene (a gift from H. Miyoshi). LVs were prepared according to the previously described method (35), except that a three-vector system was used instead of a four-vector system (36).

***In Vitro* Kinase Assay.** The *in vitro* kinase assays were performed as described (26). For the TAK1 kinase assays, endogenous TAK1 was used, and in some experiments, transiently expressed Flag-tagged TAK1 was used, with recombinant MKK6 from *Escherichia coli* as a substrate. For the NLK kinase assays, Myc-tagged NLK protein was extracted from various HepG2 cell lines expressing Myc-NLK, and subjected to the *in vitro* kinase assay to detect autophosphorylation. In some experiments, GST-$STAT3_{534-770}$ produced in *E. coli* was used as a substrate.

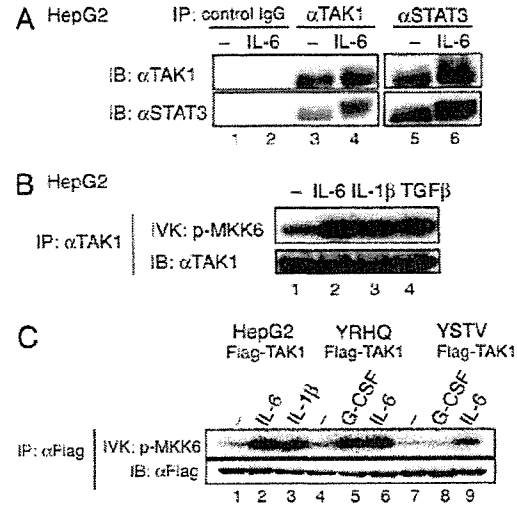

Fig. 1. Endogenous TAK1 binds to STAT3 and is activated through the YXXQ motif in gp130. (*A*) HepG2 cells were untreated ( ) or treated with IL-6 for 15 min. WCE was immunoprecipitated (IP) with control IgG (lane 1–2), anti-TAK1 (lanes 3 and 4), or anti-STAT3 (lanes 5 and 6) Abs. Immunoprecipitates were resolved on SDS-PAGE and immunoblotted (IB) with the indicated Abs. (*B*) HepG2 cells were untreated (–) or treated with 20 ng/ml IL-6, IL-1β, or TGF-β for 10 min. The proteins immunoprecipitated with anti-TAK1 Ab were divided into two aliquots. One aliquot was subjected to an *in vitro* kinase assay (IVK) with recombinant MKK6 as the substrate (*Upper*), and the other aliquot was used in an immunoblot to examine the amount of immunoprecipitated TAK1 (*Lower*). (*C*) HepG2, HepG2-G108-YRHQ, or HepG2-G108-YSTV cells were transfected with pEF-Flag-TAK1 plasmid, and untreated (–) or treated with the indicated cytokines at 20 ng/ml for 10 min. The anti-Flag immunoprecipitates of WCEs were subjected to the kinase assay (*Upper*) and immunoblot analysis with an anti-Flag Ab (*Lower*) as in *B*.

Results

Identification of TAK1 as a STAT3-Interacting Protein That Is Activated by IL-6 Through the YXXQ Motif in gp130. To identify molecules acting with STAT3, we first obtained STAT3-associated complexes by the TAP method (32) from gp130-stimulated 293T-G133 cells (4) stably expressing TAP-tagged STAT3. We analyzed digests of the complexes by using direct nanoflow liquid chromatography-coupled tandem MS (33) and identified multiple peptides. One peptide sequence, QELVAELDQDEK, corresponded to residues 521–532 of human TAK1. We then tested whether endogenous TAK1 and STAT3 formed complexes in HepG2 cells. As shown in Fig. 1*A*, lanes 3 and 4, anti-TAK1 immunoprecipitates of WCEs from unstimulated and IL-6-stimulated HepG2 cells contained STAT3. The STAT3–TAK1 interaction was reciprocally confirmed by detecting TAK1 in the anti-STAT3 immunoprecipitates (Fig. 1*A*, lanes 5 and 6).

We next tested whether IL-6 could activate endogenous TAK1. Anti-TAK1 immunoprecipitates of WCEs from unstimulated or IL-6-stimulated HepG2 cells were subjected to an *in vitro* kinase assay by using MKK6 as the substrate. As shown in Fig. 1*B*, IL-6 activated endogenous TAK1 as efficiently as did IL-1β and TGFβ. We next tested whether a tyrosine-phosphorylated motif in gp130 was required for TAK1 activation. As shown in Fig. 1*C*, stimulation of HepG2-G108YRHQ cells that express a chimeric receptor consisting of G-CSFR-gp130 with the cytoplasmic portion of gp130 truncated to 108 amino acid residues and a YXXQ motif peptide, efficiently increased the TAK1 kinase activity. In contrast, this increase was not seen in HepG2-G108YSTV cells that contain a YSTV motif instead of the YXXQ motif. These results indicated that the YXXQ motif was responsible for the TAK1 activation.

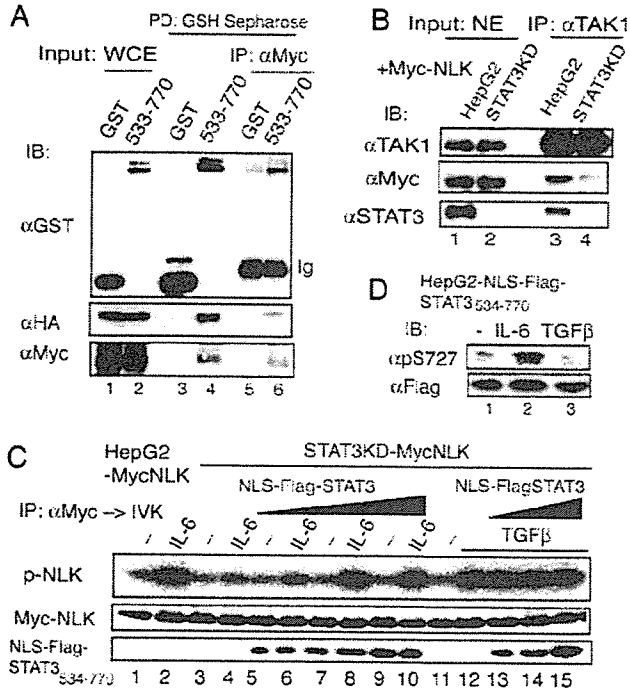

Fig. 5. The STAT3 molecule acts as a scaffold for TAK1/NLK in the YXXQ-derived pathway. (*A*) 293T cells were transfected with pCMV-HA-TAK1, pCMV-Myc-NLK, and pEFGST or pEFGST-STAT3$_{533-770}$ plasmid. The GST-labeled proteins were pulled-down with reduced glutathione (GSH)-Sepharose. The eluates were diluted with 50 mM Hepes buffer (pH 7.8) containing 150 mM NaCl, and subjected to immunoprecipitation using an anti-Myc Ab. The WCEs (lanes 1 and 2), the eluates from the GSH-Sepharose (lanes 3 and 4), and the anti-Myc Ab immunoprecipitates (lanes 5 and 6) were subjected to immunoblotting analysis with the indicated Abs. (*B*) HepG2-MycNLK and HepG2-STAT3KD-MycNLK were treated with 20 ng/ml IL-6 for 10 min. The nuclear extracts (500 μg each) were immunoprecipitated with an anti-TAK1 Ab. Nuclear extracts (20 μg, lanes 1 and 2) and the immunoprecipitates (lanes 3 and 4) were separated and probed with the indicated Abs. (*C*) HepG2-STAT3KD-MycNLK cells were infected with three doses of lentiviral preparation LV-EFNLS-FlagSTAT3$_{534-770}$. HepG2-MycNLK-, HepG2-STAT3KD-MycNLK-, and NLS-FlagSTAT3$_{534-770}$-expressing cells were stimulated with IL-6 (lanes 2, 4, 6, 8, and 10), or TGF-β (lanes 12–15) at 20 ng/ml, for 10 min or left unstimulated. The anti-Myc-immunoprecipitates (IP) of WCEs were subjected to the *in vitro* NLK kinase assay (*p*-NLK) and immunoblot (IB) with the anti-Myc Ab. (*Lower*) Immunoblots using an anti-STAT3 Ab indicate that the lysate samples contained increasing amounts of NLS-FlagSTAT3$_{534-770}$ protein in the WCE. (*D*) HepG2 cells expressing NLS-FlagSTAT3$_{534-770}$ were left untreated or treated with IL-6 or TGFβ for 15 min. The WCEs were separated on SDS/PAGE and probed with the indicated Abs.

Next, we further tested whether the interaction of endogenous TAK1 and NLK in the nucleus required STAT3 molecules. The Myc-NLK, which was expressed at a level similar to that of endogenous NLK, was located largely in the nucleus with or without IL-6 stimulation, as was endogenous NLK (Fig. 6 *B* and *C*). As shown in Fig. 5*B*, lanes 1 and 2, Myc-NLK was present at a similar level in the nuclear extracts from IL-6-stimulated HepG2-MycNLK and HepG2-STAT3KD-MycNLK cells. Comparable amounts of TAK1 were present in the nucleus (Fig. 5*B*, lanes 1 and 2) in response to IL-6, even in the absence of STAT3, and efficiently recovered with an anti-TAK1 Ab (Fig. 5*B*, lanes 3 and 4). NLK and STAT3 clearly coimmunoprecipitated with TAK1 in the nuclear extracts of IL-6-stimulated HepG2-MycNLK cells (Fig. 5*B*, lane 3), whereas the amount of NLK that coimmunoprecipitated with TAK1 in the nuclear extracts of HepG2-STAT3KD-MycNLK cells (Fig. 5*B*, lane 4) was markedly reduced to ≈15% of that in Fig. 5*B*, lane 3. These results indicate that the nuclear TAK1-NLK interaction in response to IL-6 is largely dependent on STAT3.

To substantiate this TAK1–STAT3–NLK interaction, we stably expressed an NLS-FlagSTAT3$_{534-770}$ at three different levels in HepG2-STAT3KD-MycNLK cells. These cells were left unstimulated or stimulated with IL-6 or TGFβ for 10 min, and the NLK activities were assayed. As shown in Fig. 5*C*, expression of the carboxyl terminus of STAT3 in the nucleus enhanced the IL-6-induced NLK activation in a dose-dependent manner. Interestingly, the TGFβ-induced NLK activation was not enhanced by the presence of the carboxyl terminus of STAT3 in the nucleus. These results indicate that STAT3 has an enhancing effect on the TAK1-dependent NLK activation, specifically in IL-6 signaling. We further tested whether NLK that was activated by the TGFβ signal in a STAT3-independent manner could phosphorylate STAT3 on Ser-727 in the nucleus. Very interestingly, in contrast to IL-6, TGFβ did not cause Ser-727 phosphorylation of the NLS-FlagSTAT3$_{534-770}$ expressed in the nucleus (Fig. 5*D*), suggesting that the substrate specificity of the NLKs that are activated through different pathways depends on the scaffold proteins used in the specific signaling pathways.

Discussion

This study showed that gp130, a member of the cytokine receptor superfamily, efficiently activates the TAK1 through the YXXQ motif in gp130, and this kinase preferentially activates the downstream kinase NLK, which is responsible for STAT3 Ser-727 phosphorylation via the YXXQ motif-derived signal. Furthermore, this study revealed a novel role for STAT3 in IL-6-induced NLK activation but not in TGFβ-induced NLK activation. STAT3 functions as a scaffold for TAK1 and NLK specifically in IL-6 signaling by binding them at its carboxyl-terminal region. The following observations support the idea that this interaction is physiologically significant: (*i*) most TAK1-NLK interactions in the nuclear extracts of IL-6-stimulated HepG2 cells depended on the presence of STAT3 (Fig. 5*B*); (*ii*) the IL-6-induced NLK activation was greatly decreased in HepG2-STAT3KD cells; (*iii*) STAT3 and TAK1 were independently activated by IL-6, even at low concentrations, and they then translocated into the nucleus (Figs. 4*B* and 6*A*), although most NLK resides in the nucleus before stimulation (ref. 36 and Fig. 6*B*); and (*iv*) expression of the carboxyl-terminal portion of STAT3 in the nucleus markedly increased the IL-6-induced NLK activation. In contrast, TGFβ neither used STAT3 to activate NLK (Fig. 4*B*) nor caused the phosphorylation of STAT3 on Ser-727 (Fig. 3*B*). This finding could not be explained by the fact that TGFβ did not cause the translocation of STAT3, because TGFβ-induced NLK activation could not be enhanced by the forced expression of STAT3 in the nucleus (Fig. 5*C*), and NLK activated by TGFβ did not cause Ser-727 phosphorylation of the nuclear STAT3 (Fig. 5*D*). Thus, NLKs activated through different pathways have different substrate specificities, probably reflecting the nature of the complexes containing the upstream TAK1 kinase and the scaffold proteins involved in the specific activation signals.

We previously showed that the IL-6 signals for STAT3 Ser-727 phosphorylation are mediated by at least two kinase pathways, one is a YSTV-motif-derived PD98059-sensitive pathway, and the other is a YXXQ-motif-derived H7-sensitive kinase pathway (4). The kinase pathway described here is fully consistent with the H7-sensitive kinase pathway, because it has all of the characteristics previously shown for the YXXQ-derived H7-sensitive kinase that leads to STAT3 Ser-727 phosphorylation, including the characteristics indicated in Fig. 3 *C–E*. This pathway was also active in other cell lines tested, including the NIH 3T3 and HEK293T cell lines (H. Kojima, T.S., and K.N., unpublished data). This pathway seems to be rather specific to

lentiviral vector system expressing a U6-driven loop-type small interfering RNAs against the *tak1* and *nlk* mRNAs. The LV without an RNAi sequence was used as the control. The small interfering RNAs against the *tak1* and *nlk* mRNAs effectively inhibited the production of their corresponding proteins (Fig. 3*A*). As shown in Fig. 3*B*, the YXXQ signal efficiently caused Ser-727 phosphorylation as did IL-6 at 20 ng/ml, and the YXXQ-mediated Ser-727 phosphorylation was severely impaired in both the TAK1- and NLK-depleted cells, whereas the phosphorylation of STAT3 on Tyr-705 was intact in these cells, indicating that the TAK1-NLK pathway is critical for STAT3 Ser-727 phosphorylation by the YXXQ-derived pathway. It was also noted that TGFβ did not cause STAT3 Ser-727 phosphorylation in HepG2 cells despite the strong NLK activation (Fig. 3*B*, lane 5). TAK1 kinase activity was resistant to H7 at 5 μM in the *in vitro* kinase assay (Fig. 3*C*, lanes 3 and 4), whereas the NLK kinase activity was very sensitive to H7 in the autophosphorylation kinase assay (Fig. 3*D*, lanes 1 and 2), and in an assay using GST-STAT3$_{534-770}$ made in *E. coli* as the substrate (Fig. 3*D*, lanes 3–6) with an of IC_{50} <0.1 μM. We then tested the role of this pathway in STAT3 Ser-727 phosphorylation at various IL-6 concentrations. We compared the levels of STAT3 Ser-727 phosphorylation in HepG2-G108YRHQ cells and NLK-knockdown-HepG2-G108YRHQ cells in response to increasing doses of IL-6. As shown in Fig. 3*E*, STAT3 Ser-727 phosphorylation by IL-6 was detected even at 0.1 ng/ml IL-6 and peaked at ≈ 10 ng/ml in the parental cells. In contrast, in the NLK-KD cells, the Ser-727 phosphorylation responses were suppressed when stimulated with 0.1, 0.3, and 1 ng/ml IL-6, but gradually reached a maximal level similar to that seen in the parental cells at 10 ng/ml. Very similar responses were observed in HepG2 cells pretreated with H7 at 50 μM (Fig. 3*E*, indicated as H7+) and in the HepG2-G108-TAK1KD cells (data not shown). These results indicated that the TAK1-NLK pathway actually represented the components of the previously characterized YXXQ-derived H7-sensitive kinase pathway that leads to STAT3 Ser-727 phosphorylation.

STAT3 Is Required for IL-6-Induced NLK Activation but Not for TAK1 Activation. Because STAT3 interacts with TAK1 even after IL-6 stimulation (Fig. 1*A*) and with NLK (29), we explored the role of STAT3 in the YXXQ-derived TAK1-NLK pathway. We used STAT3-knockdown HepG2 cells (HepG2-STAT3KD) and a derivative HepG2-STAT3KD cell line that was reconstituted with short interfering RNA-resistant STAT3 (HepG2-KD-STAT3R) (14). Stimulation with IL-6 at 1 and 100 ng/ml caused TAK1 activation in the HepG2-STAT3KD cells to levels comparable to those obtained in the parental cells (Fig. 4*A*, lanes 1–6). Interestingly, in response to IL-6, TAK1 translocated into the nucleus (Fig. 6*A*, which is published as supporting information on the PNAS web site), and the kinase activities in both the cytosolic and nuclear fractions increased even without STAT3 (Fig. 4*A*, lanes 7–14). These results indicated that the presence of STAT3 did not affect the activation step of TAK1 in response to IL-6.

In contrast, the IL-6-induced NLK kinase activity was markedly reduced in the HepG2-STAT3KD cells, to <20% of the activity obtained with the parental cells (Fig. 4*B*, lanes 2 and 6; see also Fig. 5*C*; average = 17.6 ± 7.2%, n = 4), and this IL-6-induced NLK activity fully recovered in the HepG2-KD-STAT3R cells (Fig. 4*B*, lanes 9 and 10), suggesting that STAT3 has a role in the TAK1-dependent NLK activation after the TAK1 activation step of the IL-6 signal. This STAT3-dependency was not observed for the NLK activation by IL-1β or TGFβ (Fig. 4*B*), indicating a specific role for STAT3 in NLK activation by IL-6 signals.

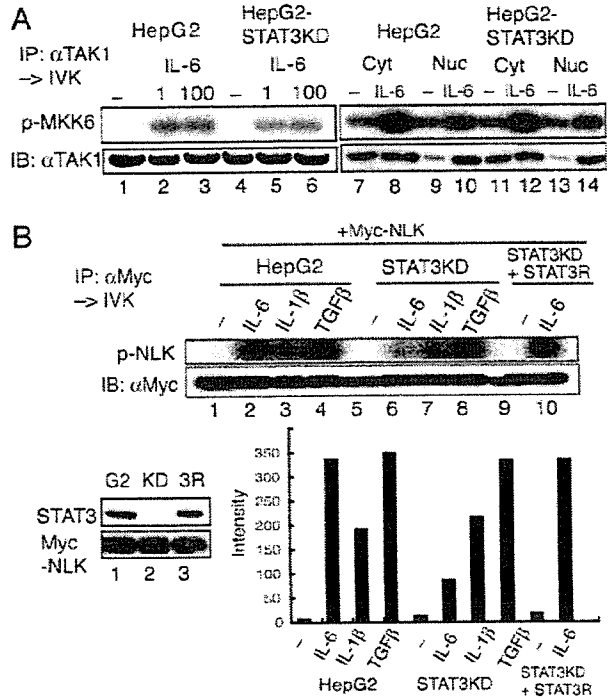

Fig. 4. STAT3 is required for IL-6-induced NLK activation but not for TAK1 activation. (*A*) HepG2 and HepG2-STAT3-knockdown (KD) cells were left unstimulated or stimulated with IL-6 at 1 (lanes 2 and 5), 100 (lanes 3 and 6), or 20 (lanes 8, 10, 12, and 14) ng/ml. Endogenous TAK1 from WCE extracts (lanes 1–6), cytosolic extracts (Cyt, lanes 7, 8, 11, and 12) or nuclear extracts (Nuc, lanes 9, 10, 13, and 14) was immunoprecipitated with an anti-TAK1 Ab, and the kinase activity was measured by using MKK6 as the substrate (*Upper*). (*Lower*) Immunoblotting with the anti-TAK1 Ab. (*B*) HepG2 (G2) cells, HepG2-STAT3KD (KD), and HepG2-STAT3KD reconstituted with RNAi-resistant STAT3 (3R) were infected with LV- Myc-NLK. The expression levels of STAT3 and Myc-NLK are shown in *Left Lower*. These HepG2 and derivative cells expressing Myc-NLK were left unstimulated or stimulated with the indicated cytokines at 20 ng/ml for 10 min. Kinase assay (*Upper*) and Western blotting analysis (*Lower*) of the anti-Myc-immunoprecipitates of WCE are shown. The radioactivity level of each band in the kinase assay was quantified with the BAS 5000 Bioimaging analyzer (Fujix, Tokyo). The activity of NLK in the IL-6-stimulated HepG2-STAT3 KD was estimated to be 17.6 ± 7.6% of that of IL-6-stimulated HepG2 cells (n = 4).

STAT3 Enhances the TAK1-Dependent NLK Activation by Acting as a Scaffold Specifically in the YXXQ-Derived Signal. We previously showed that the carboxyl-terminal region of STAT3 from residues 533 to 770 was enough to be phosphorylated on Ser-727 by the YXXQ-derived pathway (4). Consistently, GST-STAT3$_{533-770}$ fusion protein interacted with HA-TAK1 or Myc-NLK when coexpressed in 293T cells (data not shown). We then examined the nature of the interactions among STAT3, TAK1, and NLK. Glutathione beads were loaded with WCEs from cells coexpressing GST or GST-STAT3$_{533-770}$, Myc-NLK, and HA-TAK1. The protein complexes containing GST and GST-STAT3$_{533-770}$ were then recovered from the beads. As shown in Fig. 5*A*, TAK1, and NLK, interacted with GST-STAT3$_{533-770}$ (lane 4), but not with GST (lane 3). The eluates from the beads were then further immunoprecipitated with an anti-Myc Ab to obtain the NLK complexes. Anti-Myc immunoprecipitates of the eluates contained HA-TAK1 and GST-STAT3$_{533-770}$ in addition to Myc-NLK (lane 6). Control GST did not cause this coimmunoprecipitation (lane 5). Taken together with the fact that TAK1 does not directly interact with NLK (28), these results indicate that STAT3 formed a ternary complex with HA-TAK1 and Myc-NLK through its carboxyl-terminal region.

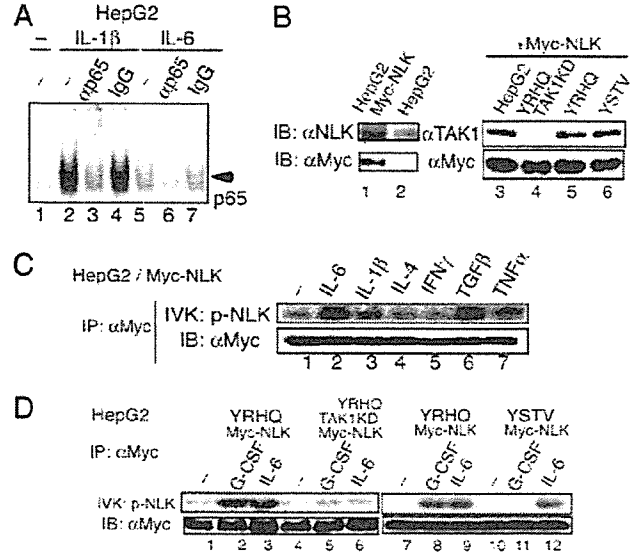

Fig. 2. Preferential activation of NLK through the YXXQ-TAK1 pathway. (*A*) EMSA for NFκB activity. ^{32}P-labeled oligonucleotides containing an NFκB-binding site and nuclear extracts from HepG2 cells that were untreated ( ) or stimulated with IL-1β or IL-6 for 30 min were used. The reaction mixtures were preincubated with no additions (lanes 1, 2, and 5), anti-p65 Ab (lanes 3 and 6), or control rabbit IgG (lanes 4 and 7). (*B*) HepG2 cells (lanes 1 and 3), HepG2-G108YRHQ (lane 5), HepG2-G108YSTV (lane 6), or HepG2-G108YRHQ with TAK1 KD (lane 4, see also Fig. 3*A*) cells were infected with LV-Myc-NLK. WCEs from parental (lane 2) and the transfected cells were immunoblotted (IB) with an anti-NLK Ab (*Left Upper*, lanes 1 and 2), an anti-TAK1 Ab (*Right Upper*, lanes 3–6) or anti-Myc Ab (*Lower*). The total amount of endogenous and exogenous NLK in the HepG2-Myc-NLK cells was estimated as ≈2- to 2.2-fold of that of endogenous NLK in the parental cells. (*C* and *D*) The various HepG2-Myc-NLK cells shown in *B* were left unstimulated or stimulated with the indicated cytokines at 20 ng/ml for 10 min. The anti-Myc immunoprecipitates (IP) of WCE were divided into two aliquots. Each aliquot was subjected to the NLK kinase assay in the absence of exogenous substrate (*Upper*) or immunoblot analysis with the anti-Myc Ab (*Lower*).

IL-6 Preferentially Activates NLK Via the YXXQ-TAK1-Mediated Pathway. Once we discovered that IL-6 activated TAK1, we investigated which downstream pathways were activated through TAK1 in response to IL-6. First, we examined NFκB activation by using an EMSA. In contrast to the efficient induction of NFκB containing p65 by IL-1β (Fig. 2*A*, lanes 2 and 3), IL-6 caused only slight NFκB DNA-binding activity in HepG2 cells (Fig. 2*A*, lanes 5 and 6). p38 and JNK activation were also tested, with no apparent activation observed in the IL-6-stimulated HepG2 cells (data not shown). We then examined whether IL-6 activated NLK. To efficiently test the NLK kinase activity, we stably expressed Myc-tagged NLK (Myc-NLK) in HepG2 cells, HepG2-G108YRHQ, or HepG2-G108YSTV, and a HepG2 cell line in which TAK1 was knocked down (described later and shown in Fig. 3*A*), with an LV expression system. The expression levels of Myc-NLK were very similar in these cell lines (Fig. 2*B*, lanes 3–6), and the level of Myc-NLK was close to that of endogenous NLK in HepG2 cells (Fig. 2*B*, lanes 1 and 2). The Myc-NLK was recovered with an anti-Myc Ab from HepG2 cells that had either been left unstimulated or stimulated, as indicated, for 10 min. The Myc-NLK was then tested for its autophosphorylation kinase activity (Fig. 2*C*). IL-6 activated NLK efficiently, as did TGFβ, IL-1β, and TNFα; two other cytokines, IFNγ and IL-4, did not activate NLK. Consistent with the role played by the YXXQ motif in the IL-6-induced TAK1 activation, stimulation of the chimeric GCSF-R-gp130 receptor containing the YXXQ motif, but not the YSTV motif, caused NLK activation at the level similar to that obtained with IL-6 (Fig. 2*D*, lanes 1–3 and 7–12). Together with the finding that the YXXQ-derived signal-induced and IL-6-induced NLK activation was severely impaired in TAK1-knockdown HepG2 cells (Fig. 2*D*, lanes 4–6), these results indicated that IL-6 preferentially activates the TAK1-NLK pathway through the YXXQ motif.

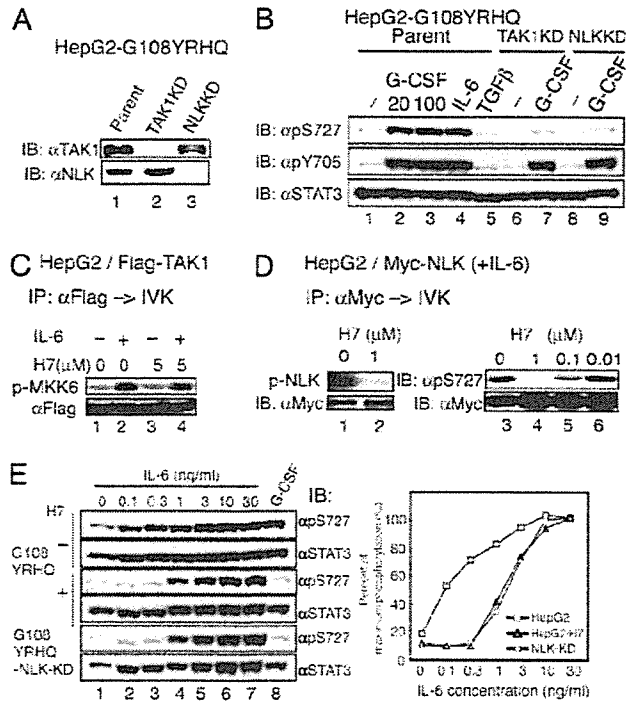

Fig. 3. TAK1 and NLK are components of the YXXQ-mediated H7-sensitive kinase pathway leading to the phosphorylation of STAT3 Ser-727. (*A*) HepG2-G108YRHQ cells were infected with LV-U6-small interfering RNA against TAK1 and NLK to deplete TAK1 and NLK (TAK1KD and NLKKD, respectively). The silencing effect was evaluated by immunoblotting with the indicated Ab. (*B*) HepG2-G108YRHQ cells and the TAK1KD or NLK KD HepG2-G108YRHQ cells were left unstimulated or stimulated with the indicated cytokines at 20 ng/ml (lanes 2, 4, and 5) or at 100 ng/ml (lanes 3, 7, and 9) for 15 min. The WCEs were immunoblotted with the indicated Abs. (*C*) The Flag-TAK1 immunoprecipitates from unstimulated or IL-6-stimulated HepG2 cells were subjected to the *in vitro* kinase assay as in Fig. 1*B* in the absence or presence of 5 μM H7. (*D*) HepG2-Myc-NLK cells were stimulated with IL-6 at 20 ng/ml for 15 min. The immunoprecipitates of WCEs with anti-Myc Ab were subjected to the *in vitro* NLK kinase assay as in Fig. 2*C* (lanes 1 and 2) or the *in vitro* NLK kinase assay by using GST-STAT3 (534–770) made in *E. coli* (lanes 3–6) in the presence of the indicated amounts of H7. Phospho-Ser-727 was detected with an anti-phospho-Ser-727 Ab (*Right Upper*). The amount of NLK used for each kinase assay is shown in *Lower*. (*E*) HepG2-G108YRHQ cells pretreated with nothing (–) or H7 at 50 μM (+) and HepG2-G108YRHQ-NLK-KD cells were left unstimulated or stimulated with the indicated concentrations of IL-6 (lanes 2–7) or 20 ng/ml G-CSF for 15 min. The WCEs were immunoblotted with the indicated Abs (*Left*). The intensities of each band were quantified by a densitometer (GS-700, Bio-Rad), and the percentage of STAT3 in the phosphorylated form was calculated (*Right*). The value in HepG2 cells stimulated with 30 ng/ml IL-6 was defined as 100%, because almost all of the STAT3 was phosphorylated on Ser-727, as judged by its migration pattern on SDS/PAGE (data not shown). Average values of two independent experiments are shown.

The TAK1-NLK Pathway Is the YXXQ-Mediated H7-Sensitive Pathway That Leads to STAT3 Ser-727 Phosphorylation. To test the roles of endogenous TAK1 and NLK in the IL-6- and YXXQ-derived signaling, we knocked down the expression levels of TAK1 or NLK in HepG2-G108YRHQ cells by the RNAi method, using a

the receptor systems that use gp130 or to others containing the YXXQ motif, because neither IFNγ nor IL-4 activated NLK. Other cytokines should be tested to see if they activate this pathway.

To date, only a few downstream targets of NLK have been identified, including TCF/LEF (26), STAT3 (ref. 29 and this study), and c-Myb (28). We do not know what other NLK substrates are in the YXXQ-derived pathway at present. Recently, Kanei-Ishii *et al.* (28) showed that TAK1, which is activated by the Wnt-1 signal, activates NLK through HIPK2, which functions as an intermediate kinase between TAK1 and NLK. NLK then phosphorylates c-Myb at multiple sites, leading to ubiquitination and proteasome-dependent degradation. In their case, c-Myb interacted with HIPK2 and NLK in the nucleus. It would be intriguing to test whether c-Myb works as a scaffold for NLK activation specifically in Wnt-1 signaling, as STAT3 appears to do in IL-6 signaling. Ohkawara *et al.* (29) showed that the TAK1-NLK pathway is responsible for the phosphorylation of *Xenopus* STAT3 on Ser-727 in the marginal zone of the 32-cell embryo, and that NLK interacts with and phosphorylates STAT3 on Ser-727 *in vitro*. Together with results showing that both STAT3 and TAK1-NLK are required for TGFβ-mediated mesoderm induction, they concluded that the TAK1-NLK-STAT3 cascade participates in the TGFβ-mediated mesoderm induction (29). However, in the present report, TGFβ did not cause STAT3 Ser-727 phosphorylation in HepG2 cells, even when the carboxyl portion of STAT3 was expressed in the nucleus, despite the strong activation of NLK by TGFβ. Clearly, more studies need to be performed to understand how different upstream pathways select the downstream kinases and affect the substrate specificity of those kinases.

We gratefully acknowledge Akihiro Iwamatsu and his laboratory for advice on protein identification. We are indebted to H. Miyoshi for the lentiviral vector system. We thank Y. Niwa for technical assistance and E. L. Barsoumian for encouraging us. This work was supported in part by the Ministry of Education, Culture, Sports, Science, and Technology of Japan, Nippon Boehringer Ingelheim Co., Ltd., GenoFunction, Inc., and the Osaka Foundation for Promotion of Clinical Immunology.

1. Levy, D. E. & Darnell, J. E., Jr. (2002) *Nat. Rev. Mol. Cell. Biol.* **3**, 651–662.
2. Decker, T. & Kovarik, P. (2000) *Oncogene* **19**, 2628–2637.
3. Wen, Z., Zhong, Z. & Darnell, J. E., Jr. (1995) *Cell* **82**, 241–250.
4. Abe, K., Hirai, M., Mizuno, K., Higashi, N., Sekimoto, T., Miki, T., Hirano, T. & Nakajima, K. (2001) *Oncogene* **20**, 3464–3474.
5. Pesu, M., Takaluoma, K., Aittomaki, S., Lagerstedt, A., Saksela, K., Kovanen, P. E. & Silvennoinen, O. (2000) *Blood* **95**, 494–502.
6. Boulton, T. G., Zhong, Z., Wen, Z., Darnell, J. E., Jr., Stahl, N. & Yancopoulos, G. D. (1995) *Proc. Natl. Acad. Sci. USA* **92**, 6915–6919.
7. Hirano, T., Ishihara, K. & Hibi, M. (2000) *Oncogene* **19**, 2548–2556.
8. Nakajima, K. & Wall, R. (1991) *Mol. Cell. Biol.* **11**, 1409–1418.
9. Nakajima, K., Kusafuka, T., Takeda, T., Fujitani, Y., Nakae, K. & Hirano, T. (1993) *Mol. Cell. Biol.* **13**, 3027–3041.
10. Ichiba, M., Nakajima, K., Yamanaka, Y., Kiuchi, N. & Hirano, T. (1998) *J. Biol. Chem.* **273**, 6132–6138.
11. Kiuchi, N., Nakajima, K., Ichiba, M., Fukada, T., Narimatsu, M., Mizuno, K., Hibi, M. & Hirano, T. (1999) *J. Exp. Med.* **189**, 63–73.
12. Yang, E., Lerner, L., Besser, D. & Darnell, J. E., Jr. (2003) *J. Biol. Chem.* **278**, 15794–15799.
13. Higashi, N., Kunimoto, H., Kaneko, S., Sasaki, T., Ishii, M., Kojima, H. & Nakajima, K. (2004) *Genes Cells* **9**, 233–242.
14. Zhao, H., Nakajima, R., Kunimoto, H., Sasaki, T., Kojima, H. & Nakajima, K. (2004) *Biochem. Biophys. Res. Commun.* **325**, 541–548.
15. Stahl, N., Farruggella, T. J., Boulton, T. G., Zhong, Z., Darnell, J. E., Jr. & Yancopoulos, G. D. (1995) *Science* **267**, 1349–1353.
16. Yamaguchi, K., Shirakabe, K., Shibuya, H., Irie, K., Oishi, I., Ueno, N., Taniguchi, T., Nishida, E. & Matsumoto, K. (1995) *Science* **270**, 2008–2011.
17. Shibuya, H., Yamaguchi, K., Shirakabe, K., Tonegawa, A., Gotoh, Y., Ueno, N., Irie, K., Nishida, E. & Matsumoto, K. (1996) *Science* **272**, 1179–1182.
18. Ninomiya-Tsuji, J., Kishimoto, K., Hiyama, A., Inoue, J., Cao, Z. & Matsumoto, K. (1999) *Nature* **398**, 252–256.
19. Irie, T., Muta, T. & Takeshige, K. (2000) *FEBS Letters* **467**, 160–164.
20. Takaesu, G., Kishida, S., Hiyama, A., Yamaguchi, K., Shibuya, H., Irie, K., Ninomiya-Tsuji, J. & Matsumoto, K. (2000) *Mol. Cell* **5**, 649–658.
21. Munoz-Sanjuan, I., Bell, E., Altmann, C. R., Vonica, A. & Brivanlou, A. H. (2002) *Development (Cambridge, U.K.)* **129**, 5529–5540.
22. Ishitani, T., Takaesu, G., Ninomiya-Tsuji, J., Shibuya, H., Gaynor, R. B. & Matsumoto, K. (2003) *EMBO J.* **22**, 6277–6288.
23. Jin, G., Klika, A., Callahan, M., Faga, B., Danzig, J., Jiang, Z., Li, X., Stark, G. R., Harrington, J. & Sherf, B. (2004) *Proc. Natl. Acad. Sci. USA* **101**, 2028–2033.
24. Moriguchi, T., Kuroyanagi, N., Yamaguchi, K., Gotoh, Y., Irie, K., Kano, T., Shirakabe, K., Muro, Y., Shibuya, H., Matsumoto, K., *et al.* (1996) *J. Biol. Chem.* **271**, 13675–13679.
25. Shirakabe, K., Yamaguchi, K., Shibuya, H., Irie, K., Matsuda, S., Moriguchi, T., Gotoh, Y., Matsumoto, K. & Nishida, E. (1997) *J. Biol. Chem.* **272**, 8141–8144.
26. Ishitani, T., Ninomiya-Tsuji, J., Nagai, S., Nishita, M., Meneghini, M., Barker, N., Waterman, M., Bowerman, B., Clevers, H., Shibuya, H., *et al.* (1999) *Nature* **399**, 798–802.
27. Ishitani, T., Kishida, S., Hyodo-Miura, J., Ueno, N., Yasuda, J., Waterman, M., Shibuya, H., Moon, R. T., Ninomiya-Tsuji, J. & Matsumoto, K. (2003) *Mol. Cell. Biol.* **23**, 131–139.
28. Kanei-Ishii, C., Ninomiya-Tsuji, J., Tanikawa, J., Nomura, T., Ishitani, T., Kishida, S., Kokura, K., Kurahashi, T., Ichikawa-Iwata, E., Kim, Y., *et al.* (2004) *Genes Dev.* **18**, 816–829.
29. Ohkawara, B., Shirakabe, K., Hyodo-Miura, J., Matsuo, R., Ueno, N., Matsumoto, K. & Shibuya, H. (2004) *Genes Dev.* **18**, 381–386.
30. Kojima, H., Nakajima, K. & Hirano, T. (1996) *Oncogene* **12**, 547–554.
31. Nakajima, K., Yamanaka, Y., Nakae, K., Kojima, H., Ichiba, M., Kiuchi, N., Kitaoka, T., Fukada, T., Hibi, M. & Hirano, T. (1996) *EMBO J.* **15**, 3651–3658.
32. Seraphin, B. (2002) *Adv. Protein. Chem.* **61**, 99–117.
33. Natsume, T., Yamauchi, Y., Nakayama, H., Shinkawa, T., Yanagida, M., Takahashi, N. & Isobe, T. (2002) *Anal. Chem.* **74**, 4725–4733.
34. Miyagishi, M. & Taira, K. (2002) *Nat. Biotech.* **20**, 497–500.
35. Miyoshi, H., Blomer, U., Takahashi, M., Gage, F. H. & Verma, I. M. (1998) *J. Virol.* **72**, 8150–8157.
36. Katayama, K., Wada, K., Miyoshi, H., Ohashi, K., Tachibana, M., Furuki, R., Mizuguchi, H., Hayakawa, T., Nakajima, A., Kadowaki, T., *et al.* (2004) *FEBS Lett.* **560**, 178–182.
37. Brott, B. K., Pinsky, B. A. & Erikson, R. L. (1998) *Proc. Natl. Acad. Sci. USA* **95**, 963–968.

Available online at www.sciencedirect.com
SCIENCE DIRECT®
DNA Repair 4 (2005) 537–545
DNA REPAIR
www.elsevier.com/locate/dnarepair

DDB2, the xeroderma pigmentosum group E gene product, is directly ubiquitylated by Cullin 4A-based ubiquitin ligase complex

Noriyuki Matsuda[a], Keiko Azuma[a,b], Masafumi Saijo[c], Shun-ichiro Iemura[d], Yusaku Hioki[d], Tohru Natsume[d], Tomoki Chiba[a], Kiyoji Tanaka[c], Keiji Tanaka[a,*]

[a] *Department of Molecular Oncology, Tokyo Metropolitan Institute of Medical Science, 3-18-22 Honkomagome, Bunkyo-ku, Tokyo 113-8613, Japan*
[b] *Department of Biology, Ochanomizu University, 2-1-1 Ohtsuka, Tokyo 112-8610, Japan*
[c] *Graduate School of Frontier Biosciences, Osaka University and Core Research for Evolutional Science and Technology (CREST), Japan Science and Technology Corporation, 1-3 Yamada-oka, Suita, Osaka 565-0871, Japan*
[d] *National Institutes of Advanced Industrial Science and Technology, Biological Information Research Center (JBIRC), Kohtoh-ku, Tokyo 135-0064, Japan*

Accepted 17 December 2004

Abstract

Xeroderma pigmentosum (XP) is a genetic disease characterized by hypersensitivity to UV irradiation and high incidence of skin cancer caused by inherited defects in DNA repair. Mutational malfunction of damaged-DNA binding protein 2 (DDB2) causes the XP complementation group E (XP-E). DDB2 together with DDB1 comprises a heterodimer called DDB complex, which is involved in damaged-DNA binding and nucleotide excision repair. Interestingly, by screening for a cellular protein(s) that interacts with Cullin 4A (Cul4A), a key component of the ubiquitin ligase complex, we identified DDB1. Immunoprecipitation confirmed that Cul4A interacts with DDB1 and also associates with DDB2. To date, it has been reported that DDB2 is rapidly degraded after UV irradiation and that overproduction of Cul4A stimulates the ubiquitylation of DDB2 in the cells. However, as biochemical analysis using pure Cul4A-containing E3 is missing, it is still unknown whether the Cul4A complex directly ubiquitylates DDB2 or not. We thus purified the Cul4A-containing E3 complex to near homogeneity and attempted to ubiquitylate DDB2 in vitro. The ubiquitylation of DDB2 was reconstituted using this pure E3 complex, indicating that DDB–Cul4A E3 complex in itself can ubiquitylate DDB2 directly. We also showed that an amino acid substitution, K244E, in DDB2 derived from a XP-E patient did not affect its ubiquitylation.

Keywords: Nucleotide excision repair; E3; Ubiquitin; DDB1; DDB2; Cullin 4A

1. Introduction

Several proteins that bind specifically to ultraviolet (UV) irradiation damaged-DNA have been discovered by electrophoretic mobility shift assay or filter-binding assay since 1970s [1]. Previous studies that have characterized the damaged-DNA binding (DDB) protein indicated that the minimal DDB complex is a heterodimer comprised of a 127 kDa DDB1 subunit and 48 kDa DDB2 subunit. The binding activity of damaged DNA is thought to reside in this heterodimeric complex (for reviews, see [2,3]).

Xeroderma pigmentosum (XP) is a rare genetic disease characterized by clinical and cellular hypersensitivity to UV radiation and high incidence of skin cancer [4]. Cells from XP patients show defective repair of DNA damage that had been induced by UV or chemical agents, and tendency for skin carcinogenesis. In 1988, Chu and Chang [5] reported that cells from XP complementation group E (XP-E) individuals (GM02415/XP2RO) lacked this damaged-DNA binding activity, suggesting that DDB is functionally involved in the XP-E disease. This is also true for some other alleles of XP-E

* Corresponding author. Tel.: +81 3 3823 2237; fax: +81 3 3823 2237.
E-mail address: tanakak@rinshoken.or.jp (K. Tanaka).

1568-7864/$ – see front matter © 2005 Elsevier B.V. All rights reserved.
doi:10.1016/j.dnarep.2004.12.012

patients [6]. Further evidence for the involvement came from microinjection experiments indicating that the purified DDB complex complements the XP-E cells' defect [7,8]. Other studies demonstrated that ectopic expression of human *DDB2* enhanced DNA repair in Chinese hamster V79 cells, which rarely express endogenous rodent *DDB2* [9]. Soon after the identification of *DDB1* and *DDB2* genes, Nichols et al. [10] revealed that *DDB2* was in fact mutated in XP-E cells lacking DDB activity. However, the molecular basis of the XP-E phenotype was ambiguous, because several groups found that cells from other patients with XP-E had normal levels of DDB activity (DDB+) and possessed no mutation in *DDB2* gene (reviewed in [2,3]). This discrepancy was puzzling until recently. Based on a thorough analysis, however, it was found that some DDB+ cell lines were mistakenly assigned to XP-E, and now it appears that all known authentic cases of XP-E are caused by *DDB2* mutations [11,12].

In eukaryotic cells, selective protein degradation is largely mediated by the ubiquitin/proteasome system. When ubiquitin is attached to the target protein by the ubiquitylation machineries, the proteasome recognizes the poly-ubiquitylated substrate to be degraded. This ubiquitin conjugating system requires the cascade reaction of three enzymes, namely E1, a ubiquitin-activating enzyme, E2, a ubiquitin-conjugating enzyme, and E3, a ubiquitin ligase. In 1999, Shiyanov et al. [13] reported that Cullin 4A (Cul4A) associates with the DDB complex. The cullin family of proteins compose a multimeric E3 complex. Cullin 1, which is the most well characterized cullin, serves as a rigid scaffold of its E3 complex and catalyses ubiquitylation through appropriate positioning of E2 and the substrate [14]. Other cullin family proteins including Cul4A are believed to function as well. The interaction between Cul4A and DDB1 was also demonstrated by several other groups recently ([15–20] and this work). These results, together with the rapid degradation of DDB2 after UV irradiation [21,22], suggest the involvement of Cullin 4A in DDB2 ubiquitylation and degradation. Strikingly, over-production of Cul4A stimulates the ubiquitylation of DDB2 [15,16]. However, since the latter studies did not show biochemical evidence of Cul4A involvement in the ubiquitylation of DDB2, it is still unknown whether the Cul4A-containing E3 complex in itself directly ubiquitylates DDB2 or not. To further investigate the mode of this ubiquitylation, an in vitro reconstitution by biochemical approach is obviously required. Here, we show that DDB2 can be ubiquitylated directly by the purified DDB–Cul4A E3 complex in a reconstitution in vitro experiment.

2. Materials and methods

2.1. Protein identification by LC–MS/MS analysis

The Cullin 4A-associated complexes were digested with *Achromobacter* protease-I and the resulting peptides were analyzed using a nanoscale LC–MS/MS system as described previously [23,24]. The peptide mixture was applied to a Mightysil-PR-18 (1 μm particle, Kanto Chemicals, Tokyo, Japan) frit-less column (45 mm × 0.150 mm i.d.) and separated using a 0–40% gradient of acetonitrile containing 0.1% formic acid over 30 min at a flow rate of 50 nl/min. Eluted peptides were sprayed directly into a quadruple time-of-flight hybrid mass spectrometer (Q-T of *Ultima*, Micromass, Manchester, UK). MS and MS/MS spectra were obtained in data-dependent mode. Up to four precursor ions above an intensity threshold of 10 counts/s were selected for MSMS analyses from each survey scan. All MS/MS spectra were searched for protein sequences of Swiss Prot and RefSeq (NCBI) using batch processes of Mascot software package (Matrix Science, London, UK).

2.2. Cell culture condition

High-Five insect cells were maintained as an adherent culture in Grace insect media (Invitrogen, Carlsbad, CA, USA) supplemented with 8% fetal bovine serum (Sigma, St. Louis, MO, USA) and 1% penicillin-streptomycin (Invitrogen). ts41 cells established from Chinese hamster [25] were maintained in Dulbecco's modified Eagle's medium (Sigma) containing 10% fetal bovine serum and 1% penicillin–streptomycin under 5% CO_2 condition at 34 °C.

2.3. Immunoprecipitation experiment

To express DDB1, DDB2 and cullin family proteins, all plasmids were constructed from pcDNA3 or pcDNA3.1 plasmid (Invitrogen). Additional details of the plasmid construction processes will be provided upon request. Mammalian ts41 cells at 48 h after DNA transfection were harvested, washed by phosphate-buffer saline (PBS) and lysed with buffer A containing 20 mM Tris–HCl, pH 7.5, 150 mM NaCl, 0.5% Nonidet P-40 and 10% glycerol. After removal of the debris by centrifugation, anti-Flag antibody (M2)-conjugated agarose (Sigma) was added to the lysate and the mixture was incubated at 4 °C for 2 h under constant rotation. After extensive washing of immunoprecipitates with buffer A, binding proteins were eluted with sodium dodecyl sulphate (SDS)-containing buffer and boiled at 95 °C for 5 min. The eluate was subjected to immunoblotting using anti-Flag (M2; Sigma), anti-Myc (Santa Cruz, Delaware, CA, USA), anti-Cul4A (our laboratory collection) and anti-DDB1 antibodies (Zymed, San Francisco, CA, USA).

2.4. Protein purification

To overproduce His-DDB1, Flag-DDB2, Cullin 4A-HA and T7-Rbx1 proteins in insect cells, the tagged full-length cDNAs were inserted into pFastBac donor plasmid (Invitrogen). Additional details of the plasmid construction processes can be provided upon request. Subsequent production of baculovirus particles was carried out according to the protocol provided by the manufacturer. Baculovirus particles for His-

DDB1 and Flag-DDB2 were used to simultaneously infect High-Five cells, as well as viruses for Cullin4A-HA and T7-Rbx1. Insect cells were incubated for 48 h after infection, washed using PBS at 4 °C and then harvested by centrifugation. The cell extract was collected using buffer B containing 20 mM Tris–HCl, pH 7.5, 0.5% Nonidet P-40, 150 mM NaCl, 100 μM $ZnSO_4$, 10 mM 2-mercaptoethanol, 6% glycerol and a protease inhibitor mixture without ethylenediaminetetraacetic acid (EDTA) (Roche, Mannheim, Germany). After centrifugation, the cell lysates were mixed together and incubated at 4 °C for 5 h with occasional gentle mixing. For initial purification, the cell lysate was loaded on a single-stranded DNA cellulose (Sigma) column equilibrated with buffer B. The column was then washed with buffer B containing 0.3 M NaCl followed by elution with buffer B containing 0.7 M NaCl. The eluted fraction was subsequently purified with nickel-chelating agarose (Qiagen, Stanford, CA, USA) pre-equilibrated with buffer B and eluted by 120 mM imidazole. This purified complex was further separated on a glycerol gradient sedimentation, which was carried out through a 10–40% glycerol gradient in 25 mM Tris–HCl, pH 7.5, 1 mM dithiothreitol (DTT) and 2 mM ATP for 22 h at 25,000 rpm ultracentrifugation. Fractions of 1 ml were collected from the top of the gradient and subjected to silver staining and immunoblotting.

To purify DDB2 (K244E)-containing complex, cell lysates containing His-DDB1, Flag-DDB2 (K244E), Cullin 4A-HA and T7-Rbx1 proteins in buffer B were collected as mentioned above. The DDB2 (K244E) complex was roughly purified with nickel-chelating agarose (Qiagen) pre-equilibrated with buffer B and eluted by 100 mM imidazole. Obtained fractions were then loaded onto HiTrap Heparin HP column (Amersham Biosciences, Piscataway, NJ, USA), washed with buffer C [20 mM Tris–HCl, pH 7.5, 150 mM NaCl, 100 μM $ZnSO_4$, 1 mM DTT, 4.5% glycerol and protease inhibitor mixture without EDTA (Roche)], and eluted with a 0.15–0.75 M NaCl gradient in buffer C. The DDB2 (K244E)-containing complex was eluted around 0.5 M NaCl and was subjected to dialysis with buffer D containing 20 mM Tris-HCl, pH 8.0, 20 mM NaCl, 100 μM $ZnSO_4$, and 1 mM DTT. A protein complex containing wild-type DDB2 was simultaneously isolated by the same method and used as a control.

To collect the authentic DDB–Cul4A complex from mammalian cells, HeLa cells stably expressing N-terminally FLAG-HA-tagged DDB2 were used. The genuine DDB–Cul4A complex was immunoprecipitated with anti-FLAG antibody followed by anti-HA antibody as described previously [17]. The eluates were further purified by Mini Q (Amersham Biosciences) column chromatography instead of glycerol density gradient centrifugation.

2.5. *In vitro ubiquitylation assay*

The ubiquitylation assay was essentially performed as described previously [26,27]. Briefly, the purified DDB–Cul4A complex was incubated in 25 mM Tris–HCl, pH 7.5, 1 mM DTT, 25 μM MG132 (Peptide Inc., Osaka, Japan), 5 mM $MgCl_2$, 100 μM $ZnSO_4$, 2 mM ATP, 50 μg of ubiquitin (Sigma)/ml, 2 μg of E1/ml and 70 μg of various E2-expressing *Escherichia coli* lysate/ml at 32 °C for 2 h and subjected to immunoblotting with anti-His (penta-His antibody; Qiagen, Stanford, CA, USA), anti-HA (HA.11, Berkeley Antibody Company, Berkeley, CA, USA), anti-Flag (M2; Sigma) and anti-T7 (Novagen, Madison, WI, USA) antibodies. In some cases, GST-ubiquitin was used instead of native ubiquitin.

3. Results

3.1. *DDB complex physically interacts with Cullin 4A*

To explore the molecular function of Cullin 4A, we examined the cellular partner(s) that interact with Cul4A in cells. A thorough analysis of human EST and genome sequences showed that the registered human Cul4A sequence (659 amino acid protein [28]) lacks its N-terminal 100 amino acid residues and thus the full-length Cul4A was obtained by PCR-assisted cDNA cloning and used hereafter. The complete nucleotide sequence of full-length Cul4A has been registered under accession number AB178950.

Flag-tagged Cul4A was expressed in HEK293 cells followed by immunoprecipitation by anti-Flag antibody. The immunoprecipitates were eluted with a Flag peptide and then digested with Lys-C endopeptides (A. protease I) and the cleaved fragments were directly analyzed using a highly sensitive "direct nano-flow LC–MS/MS" system (for detail, see Section 2). Following database search, a dozen of peptides were assigned to MS/MS spectra obtained from four nano-LC–MS/MS analyses for the Flag-Cul4A-associated complexes and DDB1 was identified as one of the Cul4A-interacting proteins.

To confirm the interaction between Cul4A and DDB1, we performed immunoprecipitation experiment. Plasmids carrying Flag-tagged cullin family proteins (Cul1, 2, 3, 4A, 4B and 5) and myc-tagged DDB1 were concurrently transfected into ts41 cells. Extracts of the transfected or mock-transfected cells were subjected to immunoprecipitation using anti-Flag antibody followed by immunoblotting with anti-DDB1 antibody. As shown in Fig. 1A, Cul4A significantly interacted with DDB1. Cul1 also bound DDB1 weakly, whereas the other Cullins tested did not interact with DDB1. We next examined whether DDB2 also associates with Cul4A, because DDB1 and DDB2 are part of the DDB complex. Plasmids carrying 6myc-tagged cullin family proteins were transfected into ts41 cells along with a plasmid harboring Flag-tagged DDB2. Each extract was then subjected to immunoprecipitation using anti-Flag antibody and immunoblotting with anti-myc antibody. Consistent with the above results, DDB2 also interacted strongly with Cul4A and weakly with Cul1 and Cul4B (Fig. 1B). DDB2 did not bind with other cullin fam-

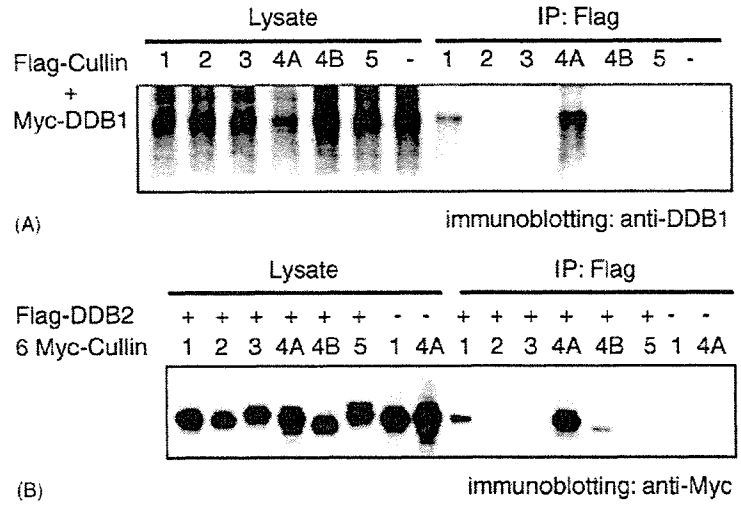

Fig. 1. DDB complex interacts with Cullin 4A. (A) Cul4A interacts with DDB1. Flag-tagged cullin family proteins and Myc-tagged DDB1 were simultaneously transfected into ts41 cells. After immunoprecipitation (IP) by anti-Flag antibody, the resulting immunoprecipitates were subjected to immunoblotting using anti-DDB1 antibody. (B) Cul4A also associates with DDB2. IP was similarly performed using FLAG-tagged DDB2 and Myc-tagged cullin family protein concurrently transfected into ts41 cells. After IP by anti-FLAG antibody, the resulting immunoprecipitates were analyzed using anti-Myc antibody.

ily proteins (Cul2, 3 and 5) examined. These results showed that DDB complex preferentially interacts with Cul4A, as reported previously [16].

3.2. Purification of DDB–Cul4A complex

We next attempted to purify DDB–Cul4A E3 complex using baculovirus expression system to perform biochemical experiments. Flag tag was fused to DDB2 at its N-terminus to facilitate its detection. This Flag-tagged DDB2 is thought to be functional because recent studies showed that ectopic expression of Flag-DDB2 enhanced DNA repair in Chinese hamster V79 cells [9], and purified Flag-DDB2 protein could restore damaged-DNA binding activity in extracts of XP-E patient cells [12]. DDB complex has been purified previously using DNA affinity column [13] and we also used DNA cellulose for initial purification of this complex. His6-tagged DDB1 and Flag-tagged DDB2 were simultaneously expressed in High-Five insect cells by the baculovirus induction system. Cul4A-HA and T7-Rbx1 were expressed concurrently as well. Each cell lysate was mixed and the resulting protein complex was purified by sequential column chromatography on single-stranded DNA cellulose, nickel-chelating agarose and subsequent 10–40% glycerol gradient by ultracentrifugation. The E3 complex comprised of DDB1, DDB2, Cul4A and Rbx1 was collected to near homogeneity as a peak fraction of glycerol gradient as shown in Fig. 2. Note that several other proteins were also detected in the final preparation (for example, a typical protein is shown by an asterisk in Fig. 2). However, since the peak fraction of such protein was inconsistent with that of the E3 complex in the glycerol gradient (data not shown), we think the protein is a contaminant derived from insect cells or a degradation product of the expressed protein, rather than a protein physiologically associated with the E3 complex.

3.3. DDB2 is ubiquitylated by purified Cul4A complex

Using this purified complex, we next tried to reconstitute the ubiquitylation of DDB2 to check whether DDB–Cul4A complex per se can ubiquitylate DDB2. Since E3 generally requires specific E2 to mediate ubiquitylation, we tested eight different E2 enzymes (E2-20k, E2-25k, Ubc3, Ubc4, UbcH5a, UbcH5c, Ubc7 and Ubc8). Slower-migrating ladders derived from auto-ubiquitylation of Cul4A (see below) were observed only from the reaction with Ubc4, UbcH5a and UbcH5c, whereas the other E2 enzymes tested did not support this modification (Fig. 3A). We thus used UbcH5 family as a source of E2 in the following experiments. Purified DDB–Cul4A complex was incubated with ATP, ubiquitin, E1 and UbcH5a, and subjected to immunoblotting with the antibody for each component. As expected, ladders derived from the auto-ubiquitylation of Cul4A were observed (Fig. 3B, single asterisk in the middle panel). Moreover, apparent high molecular-mass ladders were evident when DDB2 was detected using the anti-Flag antibody (Fig. 3B, single asterisk in the left panel). In order to demonstrate that this modification was due to ubiquitylation, we repeated the ubiquitylation assay in the presence or absence of ubiquitin. The slower migrating ladders were not detected without ubiquitin, and the addition of GST-ubiquitin instead of native ubiquitin resulted in the appearance of larger molecular-mass bands (Fig. 3B, double asterisks), indicating that this modification indeed is ubiquitylation. In the case of DDB1, a single high-molecular band also emerged after in vitro ubiquitylation (Fig. 3B, right panel). However, this ubiquitylation sig-